

Modeling of SMF tsunami hazard along the upper US East Coast: detailed impact around Ocean City, MD

Stephan T. Grilli · Christopher O'Reilly · Jeffrey C. Harris ·
Tayebeh Tajalli Bakhsh · Babak Tehranirad · Saeideh Banihashemi ·
James T. Kirby · Christopher D. P. Baxter · Tamara Eggeling ·
Gangfeng Ma · Fengyan Shi

Received: 23 February 2014 / Accepted: 2 November 2014 / Published online: 15 November 2014
© Springer Science+Business Media Dordrecht 2014

Abstract With support from the US National Tsunami Hazard Mitigation Program (NTHMP), the authors have been developing tsunami inundation maps for the upper US East Coast (USEC), using high-resolution numerical modeling. These maps are envelopes of maximum elevations, velocity, or momentum flux, caused by the probable maximum tsunamis identified in the Atlantic oceanic basin, including from far-field coseismic or volcanic sources, and near-field Submarine mass failures (SMFs); the latter are the object of this work. Despite clear field evidence of past large-scale SMFs within our area of interest, such as the Currituck slide complex, their magnitude, pre-failed geometry, volume, and mode of rupture are poorly known. A screening analysis based on the Monte Carlo simulations (MCS) identified areas for possible tsunamigenic SMF sources along the USEC, indicating an increased level of tsunami hazard north of Virginia, potentially

S. T. Grilli (✉) · C. O'Reilly · J. C. Harris · T. T. Bakhsh · C. D. P. Baxter · T. Eggeling
Department of Ocean Engineering, University of Rhode Island, Narragansett, RI 02882, USA
e-mail: grilli@egr.uri.edu

Present Address:

C. O'Reilly
Navatek Ltd., South Kingstown, RI 02879, USA

Present Address:

J. C. Harris
Saint-Venant Laboratory for Hydraulics, Université Paris-Est, 78400 Chatou, France

B. Tehranirad · S. Banihashemi · J. T. Kirby · F. Shi
Department of Civil and Environmental Engineering, Center for Applied Coastal Research, University of Delaware, Newark, DE 19716, USA

Present Address:

T. Eggeling
Delta Marine Consultants, P.O. Box 268, 2800 AG Gouda, The Netherlands

G. Ma
Department of Civil and Environmental Engineering, Old Dominion University, Norfolk, VA 2352, USA

surpassing the inundation generated by a typical 100-year hurricane storm surge in the region, as well as that from the most extreme far-field coseismic sources in the Atlantic; to the south, the MCS indicated that SMF tsunami hazard significantly decreased. Subsequent geotechnical and geological analyses delimited four high-risk areas along the upper USEC where the potential for large tsunamigenic SMFs, identified in the MCS, was realistic on the basis of field data (i.e., sediment nature and volume/availability). In the absence of accurate site-specific field data, following NTHMP's recommendation, for the purpose of simulating tsunami hazard from SMF PMTs, we parameterized an extreme SMF source in each of the four areas as a so-called Currituck proxy, i.e., a SMF having the same volume, dimensions, and geometry as the historical SMF. In this paper, after briefly describing our state-of-the-art SMF tsunami modeling methodology, in a second part, we parameterize and model the historical Currituck event, including: (1) a new reconstruction of the SMF geometry and kinematics; (2) the simulation of the resulting tsunami source generation; and (3) the propagation of the tsunami source over the shelf to the coastline, in a series of nested grids. A sensitivity analysis to model and grid parameters is performed on this case, to ensure convergence and accuracy of tsunami simulation results. Then, we model in greater detail and discuss the impact of the historical Currituck tsunami event along the nearest coastline where its energy was focused, off of Virginia Beach and Norfolk, as well as near the mouth of the Chesapeake Bay; our results are in qualitative agreement with an earlier modeling study. In a third part, following the same methodology, we model tsunami generation and propagation for SMF Currituck proxy sources sited in the four identified areas of the USEC. Finally, as an illustration of our SMF tsunami hazard assessment work, we present detailed tsunami inundation maps, as well as some other products, for one of the most impacted and vulnerable areas, near and around Ocean City, MD. We find that coastal inundation from near-field SMF tsunamis may be comparable to that caused by the largest far-field sources. Because of their short propagation time and, hence, warning times, SMF tsunamis may pose one of the highest coastal hazards for many highly populated and vulnerable communities along the upper USEC, certainly comparable to that from extreme hurricanes.

Keywords Tsunami hazard assessment · Coastal hazard · Submarine mass failure · Numerical modeling of long wave propagation · Seismic hazard

1 Introduction

Since 1995, the US National Tsunami Hazard Mitigation Program (NTHMP; <http://nthmp.tsunami.gov/index.html>) has supported the development of tsunami inundations maps for selected areas of the US coastline, based on the high-resolution numerical modeling, to allow for a better assessment and mitigation of extreme tsunami risks. Since 2009, in the wake of the devastating Indian Ocean Tsunami (e.g., Grilli et al. 2007; Ioualalen et al. 2007), this effort has been extended to include all US coastal regions. As part of this activity, the authors were tasked to develop tsunami hazard maps for the US East Coast (USEC). While a probabilistic tsunami hazard analysis (PTHA) is being planned for future phases of this NTHMP project, at present, inundation maps are being developed as the envelope of coastal inundation caused by all the probable maximum tsunamis (PMTs) in the considered oceanic basin. For the USEC, this is the Atlantic Ocean basin, in which

PMTs can be due to a variety of geological processes (or sources), including (Grilli et al. 2011): (1) far-field coseismic sources, such as caused by a M9 earthquake affecting the entire Puerto Rico Trench (PRT; e.g., Grilli et al. 2010b), or a repeat of the M8.7–8.9 1755 Lisbon earthquake in the Açores Convergence Zone (e.g., Barkan et al. 2009); (2) a far-field subaerial landslide source due to a large volcanic collapse in the Canary Islands (e.g., Abadie et al. 2012; Harris et al. 2012); and (3) near-field Submarine Mass Failures (SMFs), on or near the continental shelf break (e.g., Grilli et al. 2009; Schnyder et al. 2013). The latter SMF sources, particularly those occurring on the mainly silicate shelf of the US North East, and their potential impact on the USEC are the object of the present paper.

Although only a few historical SMF tsunamis have been clearly identified to have impacted the USEC region (e.g., Fine et al. 2005; Piper et al. 1999), ten Brink et al. (2008, 2009a, b), Chaytor et al. (2009) and Twichell et al. (2009) reported that underwater landslide scars cover a significant portion of the continental slope and rise off of the USEC; many of these landslides are old and of a large volume ($>100 \text{ km}^3$). Although seismicity is moderate along the upper USEC continental slope and upper rise of the western Atlantic Ocean (up to M7.2 earthquakes have been reported), it is sufficient to trigger large SMFs (ten Brink et al. 2008, 2009a, b; Grilli et al. 2009). While SMF tsunamis are overall less energetic than large coseismic tsunamis, they may occur in fairly shallow water at a short distance from shore and generate much more directional and focused waves, which may cause significant inundation along a narrow section of the coast (e.g., Watts et al. 2003; Grilli and Watts 2005; Watts et al. 2005; Tappin et al. 2008; Grilli et al. 2009). This warrants their analysis and modeling, together with other far-field sources, as part of the comprehensive tsunami hazard assessment we are conducting for the USEC.

Despite the clear field evidence of past large-scale SMFs within our area of interest, their magnitude, pre-failed geometry, volume and mode of rupture are poorly known. Because of this lack of data and the uncertainty in identifying locations and parameters of future potential SMFs, Grilli et al. (2009) performed a screening analysis based on the MCS, within an area initially spanning from New Jersey to Cape Cod. In the MCS, distributions of relevant parameters (seismicity, sediment properties, and SMF type, location, geometry, and excess pore pressure) were used to perform a large number of stochastic stability analyses of actual slope transects within the study area. This allowed computing statistical distributions of potential tsunamigenic SMFs, and from simplified propagation and runup computations, their expected 100- and 500-year runup. This work was later extended further south, all the way to Florida (Krauss 2011), thus identifying potential tsunamigenic SMF sources along the entire USEC area. Results of the MCS indicated an increased level of SMF tsunami hazard for return periods of 500 years north of Virginia (Fig. 1), with predictions of 5- to 6-m runup in some areas (e.g., off of Atlantic City), surpassing the inundation generated by a typical 100-year hurricane storm surge in the region. To the south, overall, SMF tsunami hazard significantly decreased.

Following this screening work, additional geophysical and geotechnical analyses were performed in areas deemed at higher risk in the MCS analysis (Eggeling 2012), to better understand the sub-bottom data, assess sediment availability, and the potential for large SMFs. This led to the identification of four areas along the upper USEC, from Virginia to Cape Cod, where the potential for large tsunamigenic SMFs identified in the MCS analysis was found to be realistic on the basis of field data (i.e., sediment nature and volume/availability) (Fig. 1). The historical Currituck slide complex (CSC), which is the largest paleoslide identified along the western Atlantic Ocean continental slope and rise, is located about 150 km south of area four (see also Fig. 2). This SMF, which occurred between 24 and 50 ka ago, when sea level was much lower, has been extensively studied from

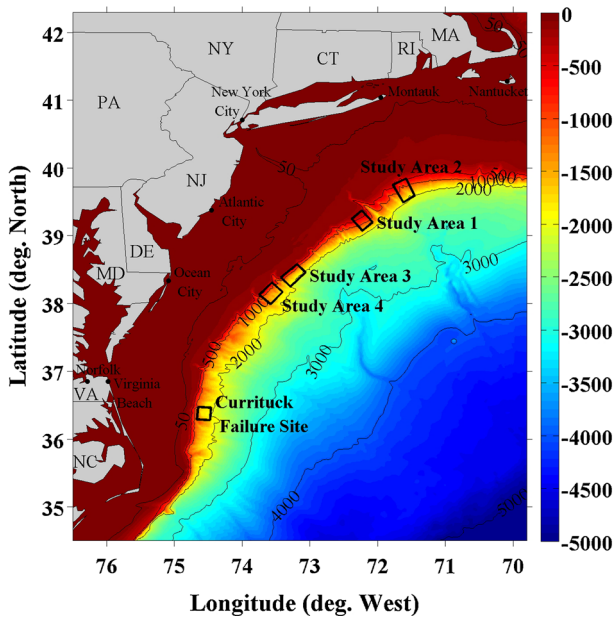


Fig. 1 Map of the region of interest in simulations of SMF tsunami hazard along the upper USEC (from Virginia to Cape Cod), with four areas (1–4) identified for potentially large tsunamigenic SMF sources (Grilli et al. 2009; Eggeling 2012). Depth is in meters, in the color scale and bathymetric contours. The historical Currituck SMF site is also marked

geological and slide triggering points of view (Bunn and McGregor 1980; Prior et al. 1986; Locat et al. 2009). Tsunami generation by a reconstituted Currituck SMF was also studied by Geist et al. (2009).

Because the NTHMP inundation mapping work done at this stage only considers the PMTs for each type of source, and in the absence of more accurate or detailed geological and geophysical field data to perform more refined slope stability analyses, it was collegially decided within NTHMP to use the parameters and geometry of the Currituck slide as a proxy for the maximum SMF tsunami that could occur along the upper USEC region, in each of the four identified areas of Fig. 1. This approach was later approved by the NTHMP Mapping and Modeling sub-committee, for the development of the first generation of tsunami inundation maps along the upper USEC, from Maryland to Cape Cod.

Accordingly, in this paper, after briefly describing in a first part our SMF tsunami modeling methodology, in a second part, we present the parameterization and modeling of the historical Currituck event, including: (1) a new reconstruction of the SMF geometry and kinematics; (2) the simulation of the resulting tsunami source generation; and (3) the propagation of the tsunami source over the shelf to the coastline, in a series of nested grids. A sensitivity analysis to model and grid parameters is performed to ensure convergence and accuracy of SMF tsunami simulation results; we also qualitatively compare our results to earlier published work for the Currituck tsunami event. Then, we model in greater detail and discuss the impact of the historical Currituck tsunami event along the nearest coastline where its energy is focused, off of Virginia Beach and Norfolk, as well as near the mouth of the Chesapeake Bay. In a third part, following the same methodology, we parameterize and model tsunami generation and propagation for four SMF Currituck proxy sources sited

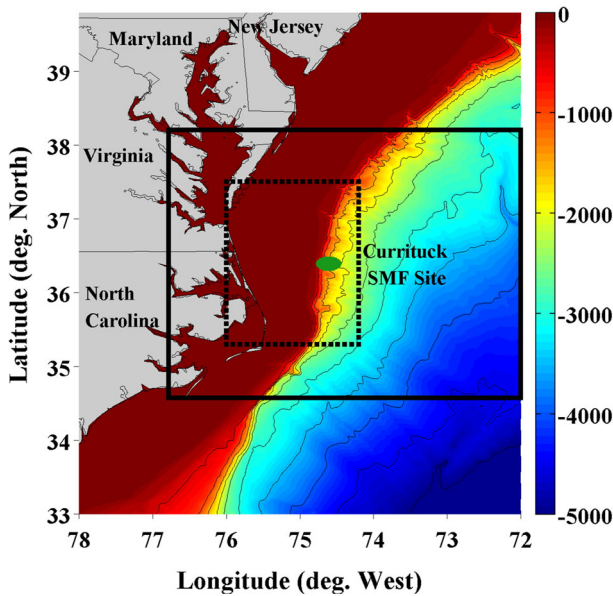


Fig. 2 Map of the area surrounding the historical Currituck SMF, with depth indicated in meters in the color scale and bathymetric contours. The *green ellipse* is the footprint of the assumed initial SMF failure (center located at 74.61W and 36.39N, where 1° in longitude is 89 km). The *solid black box* marks the boundary of the 500-m resolution grid used in NHW and FNW SMF tsunami simulations (with 800 × 900 cells and lower left corner coordinates of 76.8W and 34.6N). The *dashed black box* is a zoomed-in area used to visualize some of the simulation results (lower left corner coordinates, 76.0W and 35.3N)

in the four identified high-risk SMF areas. Finally, as an illustration of our SMF tsunami hazard assessment work, we present detailed tsunami inundation maps, as well as some other products (e.g., maps of velocity, momentum flux, and vorticity), for one of the most impacted and vulnerable areas, near and around Ocean City, MD.

2 SMF tsunami modeling methodology

2.1 SMF tsunami generation and propagation models

SMF tsunami sources are modeled in the three-dimensional (3D) non-hydrostatic model NHWAVE (Ma et al. 2012) (NHW), which has a boundary fitting σ -coordinate grid in the vertical direction and a Cartesian horizontal grid. After the SMF has stopped moving (for time $t > t_f$), surface elevation and horizontal velocity are interpolated into the nonlinear and dispersive long-wave Boussinesq model FUNWAVE-TVD (FNW), in which tsunami propagation from the source region to the various coastlines is simulated. Both Cartesian fully nonlinear (Shi et al. 2012) and spherical weakly nonlinear (Kirby et al. 2013) grid implementations are available for FNW, and simulations are performed in a series of one-way coupled nested grids, with increasingly fine resolution and commensurately accurate bathymetric and topographic data toward the coast. The rationale for this coupled modeling approach is that: (1) FNW cannot currently simulate waves generated by a moving bottom; (2) NHW can simulate a moving bottom and is 3D, hence, more accurate to simulate SMF

tsunami generation during which velocities are less uniform over depth than for the subsequent tsunami propagation (see, e.g., Grilli et al. 2002); (3) FNW is more accurate than NHW for simulating coastal wave transformations, in particular, detecting wave breaking and modeling the related dissipation, and moving shoreline algorithm; (4) FNW is more computationally efficient as it only has a 2D grid, which hence is at least three times smaller than the minimum required NHW grid to provide a similar accuracy of horizontal velocity in the vertical direction (i.e., 3 σ -layers), for an identical horizontal resolution; and finally (5) FNW also has a spherical implementation, which allows accurately simulating far-field tsunami propagation, whereas NHW only has a Cartesian horizontal grid, which limits its use to small latitudinal and longitudinal ranges.

The latter feature, however, is not used in the present paper, although combinations of spherical and Cartesian nested grids were used in earlier work (see, e.g., Grilli et al. 2013b; Kirby et al. 2013). Indeed, in the present work, because all simulations are performed in regional or nearshore grids with small latitudinal and longitudinal ranges, we only used Cartesian nested grids in FNW, with distances corrected according to a UTM type projection. This allows having undistorted grid cells nearshore, which lead to more accurate numerical results in areas with strongly nonlinear waves and many breaking zones. Additionally, because only the Cartesian implementation of FNW is fully nonlinear, it must be used anyway for the finer levels of nested grids, nearshore and on the coast, where tsunami waves become strongly nonlinear.

For each source, SMF geometry and kinematics are parameterized based on the local bathymetry and geology and used as bottom boundary conditions to force NHW simulations. NHW solves the inviscid Euler equations (viscous and turbulent effects can be included, but are neglected in the present study) with fully nonlinear free-surface boundary conditions. The model has been fully validated for both coseismic and, more importantly, rigid SMF tsunami generation and propagation, according to NTHMP and NOAA guidelines (Tehraniad et al. 2012). For long wave generation, NHW grids typically only require three vertical σ -layers, owing to the fairly uniform horizontal velocity over depth (this aspect will be verified in this paper for SMF tsunamis). FNW was also fully validated against a series of tsunami benchmarks, as part of a NTHMP Model Validation Workshop (<http://nthmp.tsunami.gov/documents/nthmpWorkshopProcMerged.pdf>; Tehraniad et al. 2011). In both models, open boundary conditions are represented by absorbing (sponge) layers. The one-way coupling method used in FNW works as follows: Time series of surface elevation and horizontal velocity are calculated in a coarser grid level, along the boundary of the next finer grid level. Computations are then restarted in the finer grid on the basis of these time series used as boundary conditions. Because reflected waves are included in the time series, the open boundary conditions are automatically satisfied between nested grids. A similar coupled modeling approach was already applied to the simulation of the coastal impact of transoceanic tsunamis along the USEC, such as from the collapse of the Cumbre Vieja Volcano in the Canary Islands (Abadie et al. 2012; Harris et al. 2012), for which the subaerial landslide tsunami source was computed using the multi-fluid 3D Navier–Stokes solver THETIS (Abadie et al. 2010). The same NHW/FNW coupling methodology was applied to simulating the coastal impact of the Tohoku 2011 tsunami, where the seismic source was specified as a time- and space-varying bottom boundary condition, to simulate tsunami generation in NHW (Grilli et al. 2013b).

In each model grid, the deepwater bathymetry is obtained from the 1 arc-min resolution ETOPO-1 data (Amante and Eakins 2009), available at NOAA's National Geophysical Data Center (NGDC) (<http://www.ngdc.noaa.gov/mgg/global/>), while nearshore bathymetry and topography are obtained from the 3 arc-sec (about 90 m) resolution NGDC

Coastal Relief Models (CRMs) (<http://www.ngdc.noaa.gov/mgg/coastal/coastal.html>) and the 1/3 arc-sec (about 10 m) NOAA-NGDC tsunami DEMs, wherever available (<http://www.ngdc.noaa.gov/mgg/inundation/tsunami/inundation.html>). All of these data sources, which have been reconciled with each other by NGDC, are seamlessly interpolated to construct model grids. Additional high-resolution DEMs for a portion of the Maryland to Cape Cod region have been obtained from ongoing FEMA hurricane and storm surge modeling efforts, but these are not utilized in the results presented here.

Both NHW and FNW have been implemented in parallel MPI FORTRAN, for an efficient solution on computer clusters with shared memory. FNW, in particular, was shown to be highly scalable, with a reduction in CPU time by about 90 % the number of processors used, as compared to a single-CPU implementation (Shi et al. 2012). In these conditions, all the simulations presented in the paper were performed on a 12 CPU (two 2.93 GHz 6-Core Intel® Xeon™ processors) Apple Desktop computer with 64 GB RAM memory, in total computational times varying between a few hours and about 22 h for the largest grids used. Clearly, on larger clusters, these CPU times could be significantly reduced.

2.2 SMF kinematics

Earlier modeling work on SMF tsunamis (Grilli and Watts 1999, 2005; Grilli et al. 2002; Lynett and Liu 2002, 2005; Watts et al. 2005) indicates that, besides volume and mean submergence depth, the initial SMF acceleration is the dominant factor for tsunami generation; hence, worst-case scenario tsunamis are typically obtained for rigid slumps (i.e., rotational landslides), in which initial acceleration is larger than for rigid translational slides, or deforming SMFs, of similar parameters. Moreover, in many cases, SMF deformation only plays a secondary role in tsunami generation, since it takes time before it significantly affects the fluid flow, and large deformations, when they occur, take place in deeper water where the SMF is no longer tsunamigenic. Hence, in the absence of more accurate field data and to be on the conservative side, for the SMF tsunami generation simulations in NHW, we assumed that both the actual Currituck slide and its four proxies failed as rigid slumps.

For rigid slumps, kinematics is specified based on the analytical laws developed by Grilli and Watts (1999, 2005), Grilli et al. (2002) and Watts et al. (2005). Additionally, as in Enet and Grilli (2007), we idealize SMF geometry as a “Quasi-Gaussian” mound of elevation ζ (whose steepness is controlled by a shape parameter ε ; here $\varepsilon = 0.717$), and elliptical footprint of length b , width w , and maximum thickness T defined as (Fig. 3),

$$\begin{aligned} \zeta(\xi, \chi) &= \frac{T}{1 - \varepsilon} \max[0, \operatorname{sech}(k_b \xi) \operatorname{sech}(k_w \chi) - \varepsilon] \\ k_b &= \frac{2}{b} \operatorname{acosh} \frac{1}{\varepsilon} \\ k_w &= \frac{2}{w} \operatorname{acosh} \frac{1}{\varepsilon} \end{aligned} \tag{1}$$

where (ξ, χ) are the local downslope and span-wise horizontal coordinates, rotated in the direction of SMF motion θ . With this geometry and parameters, the SMF volume is given by,

$$V_b = bwT \left(\frac{f^2 - \varepsilon}{1 - \varepsilon} \right) \quad \text{with} \quad f = \frac{2}{C} \operatorname{atan} \sqrt{\frac{1 - \varepsilon}{1 + \varepsilon}} \quad \text{and} \quad C = \operatorname{acosh} \left(\frac{1}{\varepsilon} \right) \tag{2}$$

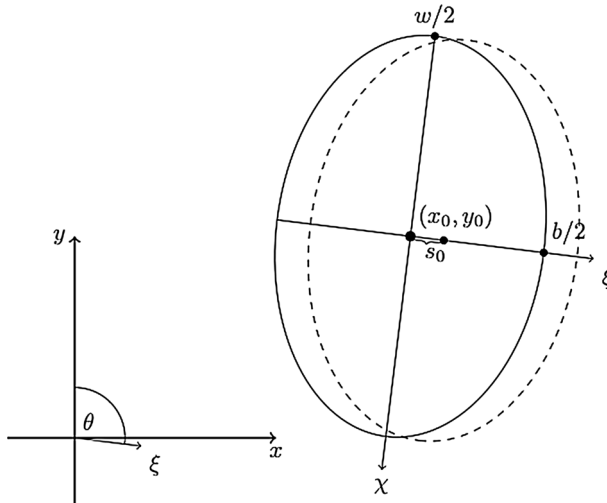


Fig. 3 Geometric parameterization of a SMF initially centered at (x_0, y_0) moving in direction ξ , with an azimuth angle θ from North and center of mass motion $s(t)$ measured parallel to the mean local slope of angle α ; (x, y) denote the longitudinal and latitudinal *horizontal* directions, respectively

Earlier modeling work (Locat et al. 2009) indicates that, during its tsunamigenic period of motion, the Currituck SMF achieved a relatively small maximum displacement (runout) $s_f < b$ in its main direction of motion down the slope, over an unknown time of motion t_f . The combination of rigid block SMF and small displacement parallel to the slope supports modeling the SMF kinematics as a rigid slump, with constant basal friction and negligible hydrodynamic drag (Grilli and Watts 2005). This type of kinematics was considered in earlier work (see above-listed references), leading to a pendulum-like center of mass motion $s(t)$ parallel to the local mean slope of angle α . In the absence of more detailed information on SMF kinematics, we will use this simple law of motion, which reads,

$$s(t) = \begin{cases} 0 & t < t_i \\ s_0 \left(1 - \cos \left\{ \frac{t - t_i}{t_0} \right\} \right) & t_i \leq t < t_i + \pi t_0 \\ 2s_0 & t_i + \pi t_0 \leq t \end{cases} \quad (3)$$

with $s_0 = s_f/2$ and $t_0 = t_f/\pi$, the characteristic time and distance of motion, respectively, and $t_i = 0$ the initial triggering time.

Unlike the simple planar slopes modeled in earlier numerical work (Grilli et al. 2010a, 2002) and in laboratory experiments (Enet and Grilli 2007), here we specify the SMF elevation over or below the actual seafloor bathymetry $h_0(x, y)$, depending on whether we reconstruct a historical failure such as the Currituck SMF (Fig. 4) or we consider a future failure (this will be detailed later for both cases). Given the initial SMF center of mass location (x_0, y_0) in global axes (x, y) (i.e., coordinates of the center of the elliptical footprint) and azimuth angle of SMF motion θ , we define the coordinate transformation to the local SMF slope-parallel coordinate system (ξ, χ) (Fig. 3) as,

$$\begin{aligned} \xi &= \{(x - x_0) \cos \theta - (y - y_0) \sin \theta\} - s(t) \cos \alpha \\ \chi &= (x - x_0) \sin \theta + (y - y_0) \cos \theta \end{aligned} \quad (4)$$

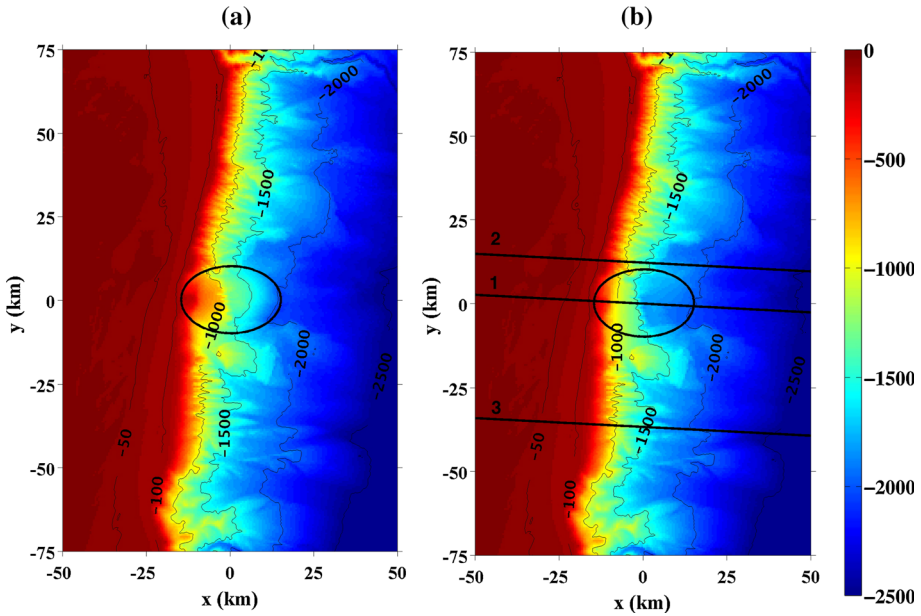


Fig. 4 Bathymetry around the Currituck SMF site. *Color scale* and bathymetric contours give depth in meters. The *ellipse* is the SMF footprint, similar to that shown in Fig. 2, and axes mark the distance measured from the SMF center (at 74.61W and 36.39N): **a** reconstructed pre-failed bathymetry; **b** current (post-failed) bathymetry with *black lines* marking bathymetric transects shown in Fig. 5. The Currituck SMF central axis corresponds to transect 1

with $s(t)$ given by Eq. (3) [Note that, since Currituck is a historical event, in the modeling, $h_0(x,y)$ must be the pre-failed bathymetry and not the current one. This requires first reconstructing pre-failed conditions, which is detailed in the next section. Then, the instantaneous seafloor depth above the SMF is given by,

$$h(x, y, t) = h_0(x, y) + \zeta \{ \xi(x, y, t), \chi(x, y) \} - \zeta \{ \xi(x, y, t_i), \chi(x, y) \} \tag{5}$$

with $\Delta h = h - h_0$. The seafloor motion described by Eq. (5) is similar to a horizontal translation downslope of part of the seabed, while accounting for actual bathymetry. The vertical seafloor velocity (also used in NHW as a bottom boundary condition) is then computed as,

$$\frac{dh}{dt}(x, y, t) = \frac{d}{dt} \{ \zeta \{ \xi(x, y, s(t)), \chi(x, y) \} \} \tag{6}$$

which can be easily derived from Eqs. (1–5).

For rigid slumps, hydrodynamic drag can be neglected due to low velocity and small amplitude of motion, and inertia includes both the SMF mass $M_b = \rho_b V_b$, with ρ_b denoting the bulk density and the specific density being defined as $\gamma = \rho_b / \rho_w$, with ρ_w the water density, and an added mass $\Delta M_b = C_m \rho_w V_b$, defined by way of an added mass coefficient C_m . Assuming a constant basal friction, a nearly circular rupture surface of radius R , and a small angular displacement $\Delta \phi$, Grilli and Watts (2005) derived the characteristic distance and time of motion for rigid slumps as,

$$s_0 = \frac{R\Delta\phi}{2} \text{ and } t_0 = \sqrt{\frac{R\gamma + C_m}{g(\gamma - 1)}} \text{ with } R \cong \frac{b^2}{8T} \quad (7)$$

with g denoting the gravitational acceleration. The last Eq. (7), proposed by Watts et al. (2005), is a semi-empirical relationship to estimate the radius of slump motion as a function of slump downslope length and maximum thickness.

3 Simulation of the Currituck SMF Tsunami generation, propagation and coastal impact

Tsunami generation and propagation for the historical Currituck SMF event was modeled by a few authors, including Geist et al. (2009) who used the dispersive weakly nonlinear Boussinesq model COULWAVE. They extracted the SMF geometry from the bathymetry and specified its motion as a bottom boundary condition (Lynett and Liu 2002, 2005), based on a rigid slide kinematics similar to that proposed by Grilli et al. (1999, 2002, 2005), although details are lacking. They simulated the Currituck tsunami (2D) wave field using a range of potential SMF movements (i.e., vertical displacement and duration of motion), bounded by the mobility analysis of Locat et al. (2009), and studied the effects of slide duration (from $t_f = 7.2$ to 20 min, with the most realistic duration being 10 min) and bottom friction coefficient ($C_d = 0.001$ – 0.01 , with the most realistic value being 0.0025; note, C_d is a non-dimensional coefficient used in a standard quadratic bottom shear stress formulation) on tsunami generation and propagation. Additionally, a high-resolution (5-m grid) fully nonlinear simulation was performed along a one-dimensional E-W transect, highlighting the importance of wave breaking, dispersion, and nonlinearity on near shore propagation; however, no detailed nearshore tsunami impact was computed. Geist et al.'s results indicate that, for a given bottom friction coefficient, nearshore runup is primarily affected by SMF volume and then by failure duration (i.e., slide acceleration), which is consistent with earlier findings (e.g., Grilli and Watts 2005).

3.1 Modeling of the Currituck SMF geometry

Detailed descriptions of the stratigraphy and morphology of the Currituck SMF have been reported on the basis of seismic surveys by Bunn and McGregor (1980), Prior et al. (1986), and Locat et al. (2009). The latter work in particular presents a morphostratigraphic model of the failed mass and a depositional model of the runout zone, based on which the salient tsunamigenic characteristics of the Currituck SMF can be inferred (see, Locat et al.'s Figs. 3, 4). Thus, we find that the Currituck event consisted of two separate failed masses: Slide 1, which had an $\sim 100 \text{ km}^3$ volume of sediment and Slide 2, which had a $\sim 60 \text{ km}^3$ volume and that the failure occurred fairly rapidly. This justifies that, for the purpose of tsunami generation, the Currituck SMF be modeled as a single failed mass.

Based on these geological analyses, we located the center of mass of the pre-failed Currituck SMF at $x_0 = 74.7\text{W}$ and $y_0 = 36.5\text{N}$ (Fig. 2), in a 1,800 m depth, and assumed it had a maximum downslope length $b = 30 \text{ km}$ and width $w = 20 \text{ km}$ (Fig. 3), with a maximum thickness of roughly $T = 750 \text{ m}$ close to the center of the failed area. With these dimensions, Eq. (2) yields a volume of failed sediment, $V_b = 134 \text{ km}^3$, which is in reasonable agreement with past geological work, in which slide volume was estimated to $V_b = 128$ – 165 km^3 (Prior et al. 1986). The headwall of Slide 2 begins at an approximate

500 m depth and is about 200 m thick; we assumed that this headwall roughly marks the shallower boundary of the failed area, which constraints the pre-failed SMF horizontal footprint (Fig. 4a). Although parts of the SMF traveled for large distances on the seafloor, to establish the SMF kinematics relevant to tsunami generation, we will only consider and parameterized the runout distance (and related time of motion) corresponding to the so-called tsunamigenic part of SMF motion; this is detailed later. Finally, based on the literature and on the seafloor morphology, we assumed that the SMF traveled due East, i.e., in azimuthal direction $\theta = 90^\circ$, which is nearly perpendicular to the isobaths.

3.2 Currituck SMF geometry/bathymetry reconstruction

The pre-failed bathymetry of the Currituck SMF is reconstructed by adding the sediment volume V_b to the post-failed area. However, a direct addition of the SMF geometry described by Eq. (1) to the current bathymetry would not accurately reconstruct the failed slope as it was determined that, during its motion, the failed sediment from Slide 2 moved (flowed) into and partially filled the back of the cavity left by Slide 1 (Prior et al. 1986). Therefore, part of the sediment within the reconstructed Currituck SMF should consist of sediment currently found at the site (i.e., sediment having flowed from Slide 2 into the back of Slide 1 after the main tsunamigenic period of motion). To account for this, after some trials and error, we first removed a $T = 250$ m thick SMF from the post-event site [also described by Eq. (1) and with the same width and length as the full SMF; Fig. 5 transect in dashed red]. The pre-failed bathymetry used in NHW simulations was finally obtained by adding the full SMF volume and geometry, with maximum thickness $T = 750$ m to this modified transect (solid black transect in Fig. 5); at its center, the pre-failed SMF is now in a $d = 1,300$ m depth.

Figure 5 illustrates the SMF pre-failed bathymetry reconstruction and compares it to the surrounding area. Although the Currituck pre-failed bathymetry and geometry (assumed Quasi-Gaussian here) are unknown, the bathymetry of the surrounding continental slope can be used as a first approximation to validate our reconstruction. Thus, Fig. 5 compares the current bathymetric transects 2 and 3 (marked in Fig. 4b), which pass through areas north and south of the failure site, to transect 1, which passes through the center of the reconstructed Currituck SMF bathymetry, before and after reconstruction. We see that transects 2 and 3 are consistent with each other and that the reconstructed pre-failed

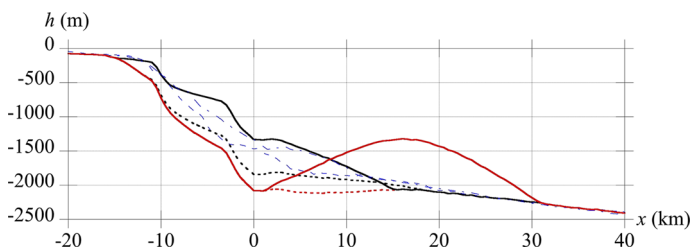


Fig. 5 Bathymetric transects through and adjacent to the center of the Currituck slide, marked in Fig. 4: (short dash curve) current post-failed bathymetry along the SMF direction of motion (transect 1); current post-failed bathymetry along transects 2 (long dash curve) and 3 (long and short dash curve); (black solid curve) reconstructed pre-failed bathymetry along transect 1; (red short dash curve) transect 1 bathymetry with a Currituck SMF of 250 m maximum thickness removed; and (red solid curve) transect 1 bathymetry at the end of the SMF tsunamigenic motion duration (at time $t = t_f$), computed with Eqs. (3–5)

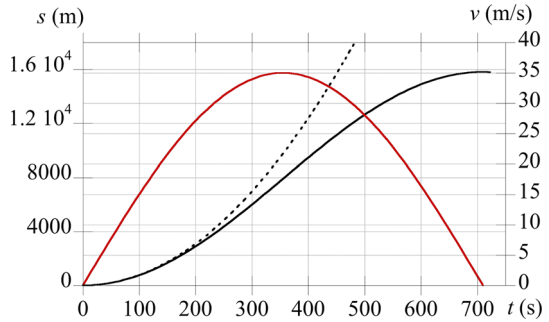
transect 1 is consistent with both of these, confirming that reconstruction is relevant. Further improvements could be achieved by adding a few small canyons, but these would likely be inconsequential for tsunami generation (Locat et al. 2009). Finally, it should be pointed out that transect 1, shown in Fig. 5, only predicts the bathymetry at the end of the tsunamigenic part of SMF motion (estimated in the next section to last for about 12 min). Beyond this time, based on earlier work (Locat et al. 2009), the mound of failed sediment (shown between 0 and 30 km in the Fig. 5) is expected to keep spreading out in all directions, mostly downslope but also upslope in the back of the SMF to fill part of the initial small cavity that was removed prior to adding the SMF volume. However, based on earlier work (e.g., Grilli and Watts 2005; Abadie et al. 2012), wave generation due to this spreading motion in very deep water is expected to be small. Grilli and Watts (2005) (and others such as Geist et al. 2009) indeed showed that initial acceleration and short-term motion of fairly rigid SMFs are responsible for most of the tsunami generation. Abadie et al. (2012), who modeled a strongly deforming partly submerged and partly subaerial slide, by performing a detailed analysis of energy exchanges between the SMF debris flow and fluid motion, showed that the tsunamigenic part of SMF motion only lasted for a short time. A thick near-bottom debris flow propagated for a long time after the initial tsunamigenic motion, but it essentially induced a recirculation of failed material onto itself, with very little additional energy conveyed to the water motion and hence negligible wave generation; in any case, additional wave generation if any, as a result of this debris flow, would only add to the offshore propagating waves and not to the tsunami directed onshore, which is the object of the present work.

3.3 Detailed Currituck SMF kinematics

The Currituck SMF is modeled as a rigid slump, with geometry described by Eqs. (1–2) and kinematics by Eqs. (3–6), both of which are specified as bottom boundary conditions in NHW simulations. Assuming $\gamma = 1.85$ and $C_m = 1$, as in Grilli and Watts (2005), Eq. (7) yields $R = 150$ km and a characteristic time of motion $t_0 = 226$ s, resulting in a failure duration $t_f = 11.9$ min, which is consistent with the likeliest duration of 10 min proposed by Geist et al. (2009) (although their law of motion and slide displacement were quite different). This duration is also consistent with that of the tsunamigenic slide motion inferred from the slide velocity profiles calculated by Locat et al. (2009) (shown in their Fig. 14a). They used two types of deforming slide models (Bingham and Bilinear) to calculate the velocity of the Currituck SMF frontal element. On this basis, they concluded that the peak slide velocity during the event was likely between 30 and 40 m/s. Since the distance traveled by the Currituck SMF during the tsunamigenic part of its motion is unknown, we selected the slide runout s_f and characteristic distance traveled s_0 such that, with the above t_0 value, the maximum slump velocity predicted by Eq. (3) would match that of Locat et al. (2009), i.e., $v_{\max} = s_0/t_0 \approx 35$ m/s. This yields $s_0 = 7,910$ m, $s_f = 15.8$ km (Fig. 6), and $\Delta\phi = 0.11$ rad or 6.0° , which is consistent with the assumed small angular displacement of the rigid slump theory; finally, the SMF initial acceleration is $a_0 = s_0/(t_0)^2 = 0.155$ m/s². The bathymetry, computed using Eqs. (3–5) at the end of tsunami generation at $t = t_f$, is shown in Fig. 5 (solid red transect). Beyond this point, the SMF would have reached the lower velocity and acceleration region described by Locat et al. (2009), assumed to be zero (i.e., negligible for tsunami generation) here (Fig. 6), and would disperse over the seafloor without additional tsunamigenic effects.

It should be noted that this simplified pendulum-like slump kinematics $s(t)$ represents the SMF displacement parallel to the average slope α , which for a small angular

Fig. 6 Currituck SMF (slump) motion $s(t)$ (black solid curve) (and velocity $v(t)$ (red solid curve) as a function of time t (Eqs. 3–6), used to specify the bottom boundary condition in NHW simulations; (short dash curve) simple accelerating law of motion: $s(t) \approx 0.5 a_0 t^2$



displacement $\Delta\phi$ is identical to a small circular arc, or chord, along a circle of radius R . Grilli and Watts (2005) and Watts et al. (2005) showed that, for rigid SMFs, during the initial accelerating part of the motion, when the SMF is most tsunamigenic, whether assuming a slide or a slump motion, the kinematics can be approximated by, $s(t) \approx 0.5 a_0 t^2$. This simplified accelerating law of motion is marked in Fig. 6, and we see that up to $t = t_0$, differences are quite small with Eq. (3) (8 % difference at this time). For later times, the slump is gradually decelerated by gravity and basal friction, until it stops for $t = t_f$; a slide, by contrast, would reach a terminal velocity on the slope, when hydrodynamic drag and basal friction will balance inertia and gravity forcing and further decelerate when reaching the abyssal plain.

3.4 Simulation of the Currituck tsunami source generation and early propagation

3.4.1 Simulation of SMF tsunami source generation with NHW

Generation of the Currituck SMF tsunami source is simulated with NHW up to at least $t_f = 710$ s (11.9 min.), during which time bottom boundary conditions are specified based on the geometry, bathymetry, and slump-like kinematics discussed in the previous sections (Fig. 6; Table 1). We first use a 3D NHW grid with 3 σ -layers, and a 500-m resolution Cartesian horizontal mesh; the grid as a horizontal footprint of 450 by 400 km (900×800 cells), which is shown in Fig. 2. The figure also shows a smaller area of 165.5 by 244 km, over which we zoom-in to better visualize results in some of the following figures. A sensitivity analyses detailed later will confirm that a 500-m resolution with 3 σ -layers is adequate to ensure convergence of the present simulations with NHW. Finally, to maximize tsunami generation, we assumed that there is no hydrodynamic bottom friction in NHW at this initial stage of simulations (i.e., $C_d = 0$).

Figure 7 shows instantaneous surface elevations computed in NHW at four different times, up to 800 s (13.3 min.), i.e., slightly after the slump has stopped moving (at $t_f = 710$ s). In Fig. 7d, after the tsunamigenic duration of motion, surface elevations are large and range between approximately -20 and $+20$ m. Figure 8 shows surface elevations computed along an E-W transect through the SMF center, for these and other results obtained at later times, up to 2,000 s (33.3 min.). More specifically, Figs. 7 and 8 show that, at 125 s after initiation of slide motion, the SMF source surface elevation takes the form of two inverted quasi-Gaussian humps located symmetrically above the initial slide location ($x = 0$). This is qualitatively consistent with earlier results of fully nonlinear potential flow computations for rigid SMFs of idealized shape moving down a plane slope,

Table 1 Parameters [see Eqs. (1–7) for parameter definitions] of the actual Currituck SMF and of SMF proxies used in selected study Areas 1–4 (Figs. 1, 21), and horizontal footprint of grids used in NHW simulations of SMF sources

SMF and grid	Currituck SMF	Study area 1	Study area 2	Study area 3	Study area 4
Grid lg. N (km)	400	500	500	500	500
Grid lg. E (km)	450	500	450	500	500
Grid SW corner	34.6N, 76.8W	36.5N, 74.6W	36.9N, 73.9W	35.7N, 75.5W	35.4N, 75.9W
SMF T (m)	750	750	750	750	750
SMF b (km)	30	30	30	30	30
SMF w (km)	20	20	20	20	20
Avg. slope α (°)	4	4	4	4	4
SMF center of mass (x_0, y_0)	36.39N, 74.61W	39.19N, 72.19W	39.76N, 71.49W	38.41N, 73.19W	38.09N, 73.60W
θ (° North)	90	136	153	140	126
s_f (km)	15.8	15.8	15.8	15.8	15.8
t_f (s)	710	710	710	710	710

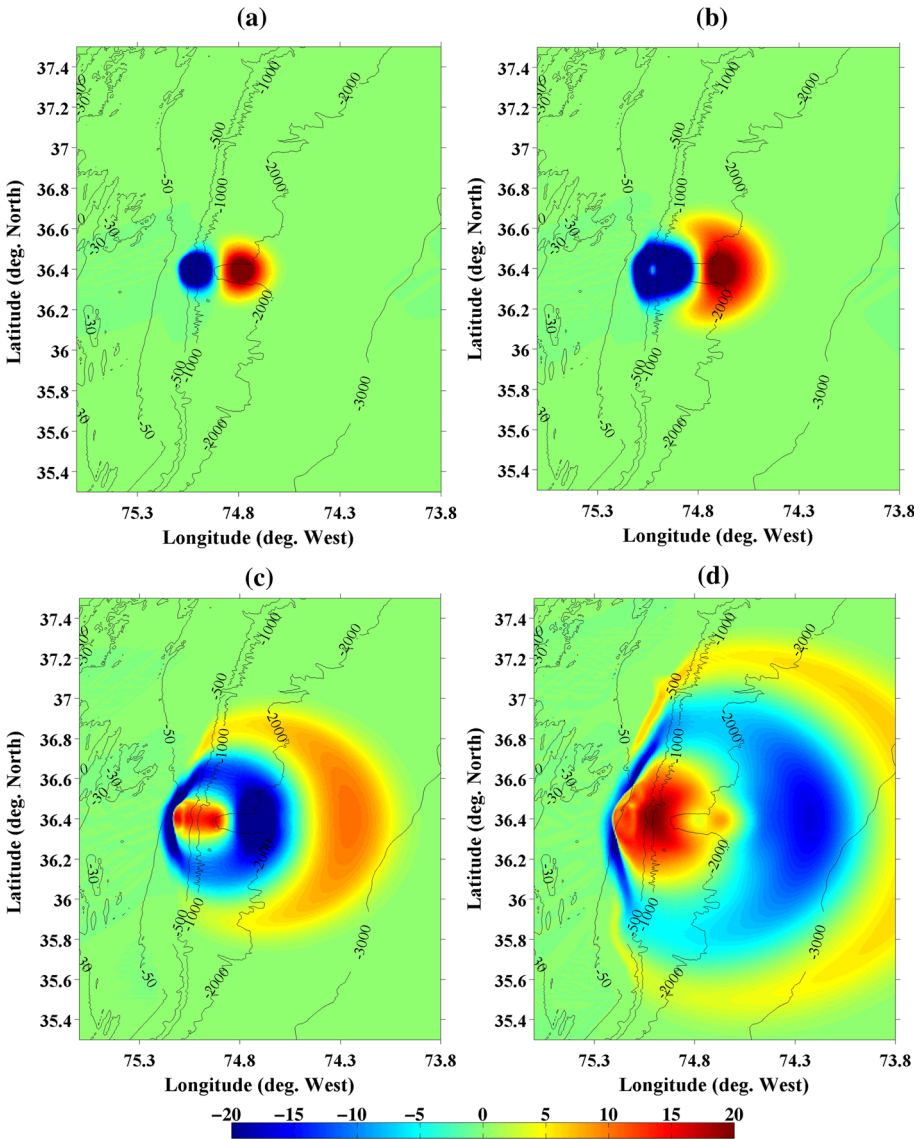


Fig. 7 Currituck SMF tsunami source generation in NHW ($C_d = 0$; 500-m resolution grid, 3 σ -layers). Instantaneous surface elevation (*color scale* is in meter) at: **a** 125 s; **b** 250 s; **c** 500 s; and **d** 800 s (13.3 min.) after SMF triggering (see Fig. 8 for E-W transects through these results). Bathymetric contours are marked in meters

reported by Grilli et al. (1999, 2002, 2005, 2010a) and Watts et al. (2005). Between 250 and 800 s, the same figures show that the initial negative elevation wave propagates onshore, together with a new “rebound” wave crest that appears within its trough. Both of these waves later shoal-up and transform through interactions with the continental shelf slope and cause onshore tsunami impact; this incoming wave train thus initially looks like a so-called N-wave (Fig. 8, curves b, c).

During the same time period, the positive (Quasi-Gaussian) elevation wave, initially generated in deeper offshore waters, propagates further offshore as a cylindrical wave crest of decreasing elevation. Among those waves, the larger elevation (10–15 m) waves near the SMF main eastern direction of motion keep propagating offshore toward the far field. The smaller elevation (5–7 m) waves to the north, however, start refracting over the shelf slope and propagating toward the Delaware Bay (Fig. 7d); this was also observed in Geist et al.'s (2009) qualitatively similar simulations and will be further detailed later when performing a computation in a larger domain. This overall pattern of wave generation is fully consistent with earlier modeling work by Grilli et al. (2002, 2010a) for idealized SMF geometry and bathymetry and confirms that the main onshore propagating tsunami is mainly a result of the initial surface depression, which is fully generated around $t = t_0$ (see Fig. 7b and curve b in Fig. 8a), hence, during the accelerating phase of the SMF motion (Fig. 6); this also confirms that any subsequent wave generation due to near-bottom debris flows occurring for $t > t_f$, if any, would not contribute to the onshore propagating tsunami waves.

During its interactions with the continental shelf slope, both shoaling and reflection of the onshore propagating tsunami N-wave occur, as well as directional spreading (see results at 500 and 800 s in Figs. 7 and 8). At 800 s (13.3 min.), the maximum wave elevation reaches about 20 m offshore. For later times (Fig. 8, curves e to h), as waves propagate further onshore and over the shelf edge, the maximum height (trough to crest) of the incoming N-wave first stays near the same value (with shoaling compensating the decay due to directional spreading), reaching 19 m over the shelf at $t = 1,100$ s, in a depth of 40 m, before it starts decreasing as the wave more strongly spreads out laterally (see

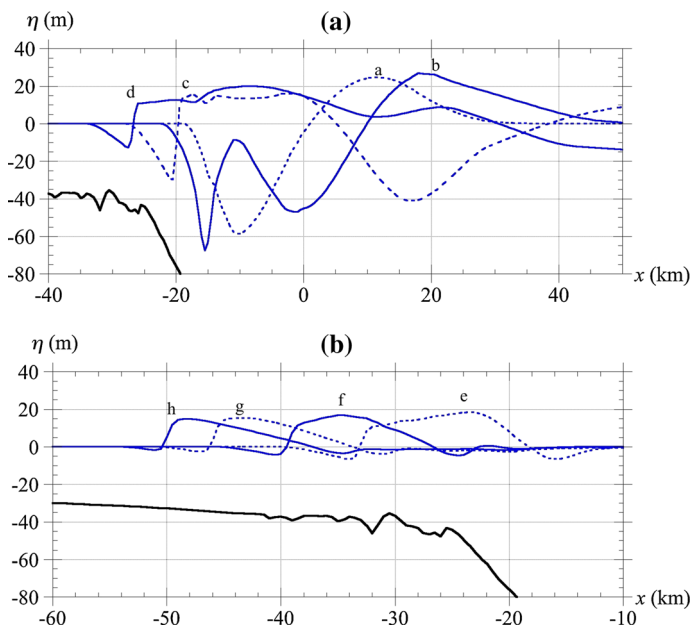


Fig. 8 Instantaneous surface elevations (solid curve, short dash curve) in NHW simulations of the Currituck SMF tsunami ($C_d = 0$; 500-m resolution grid, 3 σ -layers), at: **a** 125 s; **b** 250 s; **c** 500 s; **d** 800 s (13.3 min); **e** 1,100 s; **f** 1,400 s; **g** 1,700 s; and **h** 2,000 s (33.3 min) after SMF triggering. Results are shown along an E-W transect through the SMF center (36.39N lat.), as a function of the distance to the center of the SMF; (thick solid curve) denotes the ocean depth

results up to $t = 2,000$ s here and in Fig. 9). This decay in elevation will be enhanced by dissipation, first due to bottom friction and later to breaking, both of which will be modeled in FNW increasingly finer nested grids, when simulating tsunami propagation over the shelf (see results in a following section).

3.4.2 Convergence of NHW results

Here, we verify that the generation of the Currituck SMF tsunami source in NHW is sufficiently accurate (i.e., converged) in a 500-m resolution grid with 3 σ -layers in the vertical direction. To do so, we compare these results to those obtained in a 500-m resolution grid with 5 σ -layers and in a 250-m resolution grid with 3 σ -layers, thus assessing changes due to a finer vertical or horizontal discretization. Once NHW convergence is assessed in a 500-m resolution grid with 3 σ -layers, these model parameters

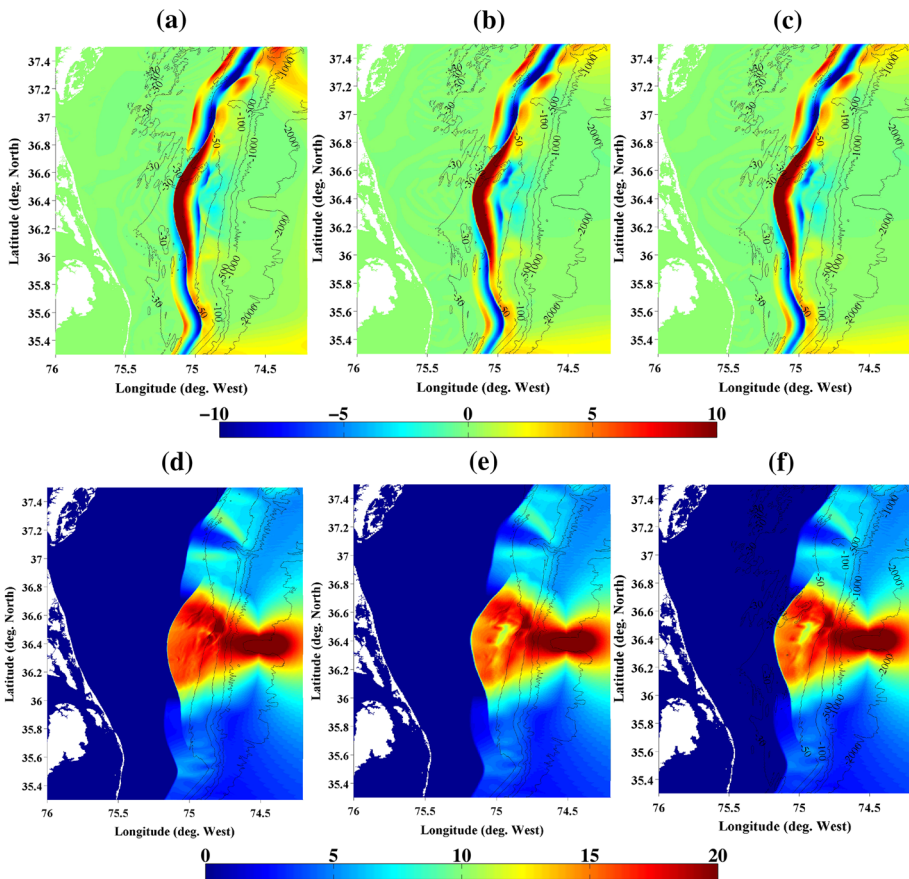


Fig. 9 Instantaneous (a, b, c) and maximum (d, e, f) surface elevation (*color scales* are in meters) at $t = 2,000$ s (33.3 min.) after SMF triggering in NHW simulations of the Currituck SMF tsunami ($C_d = 0$; same case as in Figs. 7 and 8), using: a, d a 250-m resolution grid with 3 σ -layers; b, e a 500-m resolution grid with 5 σ -layers; or c, f a 500-m resolution grid with 3 σ -layers. Results are shown in the zoomed-in area of Fig. 2; bathymetric contours are marked in *meters*

will be used in simulations of tsunami generation for Currituck SMF proxies specified in each of the four selected areas along the USEC (Fig. 1).

Results of NHW's convergence study are first shown in Fig. 9, in the form of both instantaneous and maximum surface elevations computed at $t = 33$ min, in the three tested grids configurations. The agreement between all results is very good, as can be more easily assessed in Fig. 10, in an E-W transects through the center of the SMF of surface elevations computed at $t = 33$ min in the three grids. Figure 10a shows that refining the horizontal grid resolution by a factor of 2 yields very similar surface elevations, but introduces a slight time shift in results (i.e., waves appear to be slightly slower in the finer grid likely

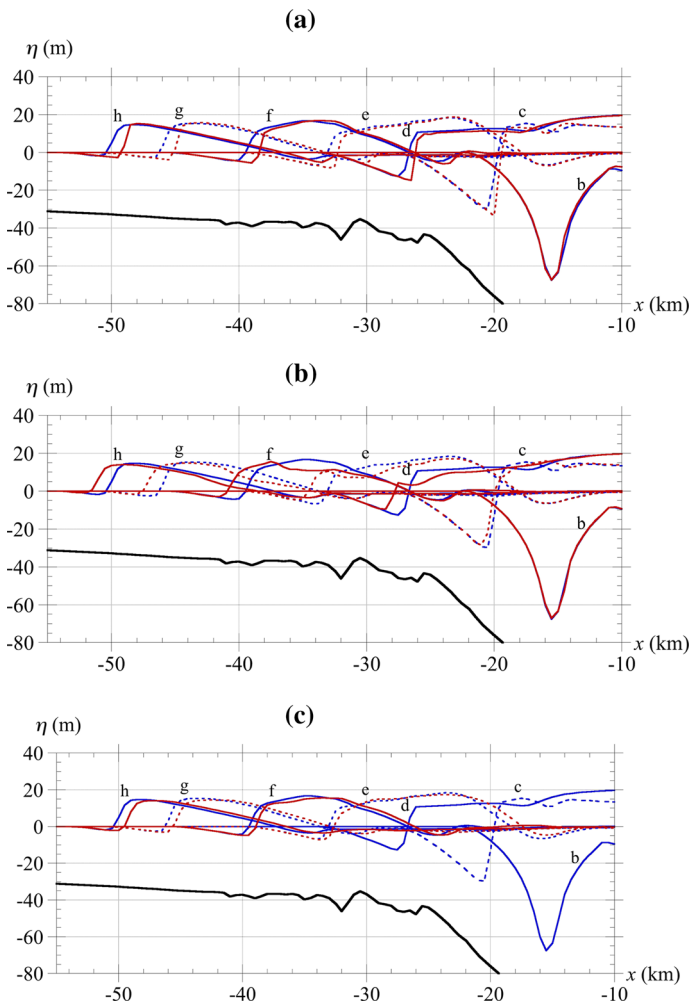


Fig. 10 Comparison of NHW (500 m, 3 σ -layers) surface elevations of Fig. 8 (blue solid curve, blue short dash curve) with those of (red solid curve, red short dash curve): **a** NHW in a 250-m resolution grid with 3 σ -layers; **b** NHW in a 500-m resolution grid with 5 σ -layers; **c** FNW in a 500-m resolution grid initialized with NHW 500-m resolution grid results at 800 s (13.3 min). We use $C_d = 0$, and results are shown along an E-W transect through the SMF center (36.39N lat.), as a function of the distance to the center of the SMF

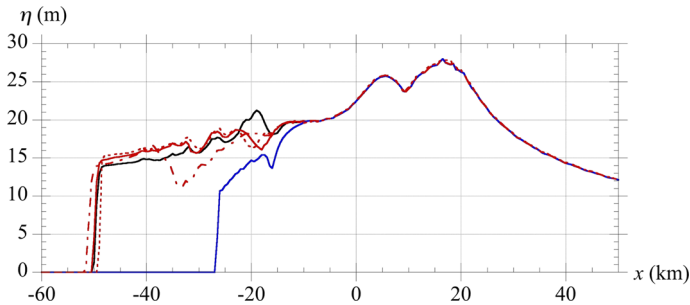


Fig. 11 Maximum surface elevation in simulations of the Currituck SMF tsunami ($C_d = 0$), along an E-W transect through the SMF center (36.39N lat), as a function of the distance to the center of the SMF, at: (blue solid curve) 800 s (13.3 min) in NHW 500-m resolution grid with 3 σ -layers (Fig. 7); and 2,000 s (33 min) in FNW 500-m resolution grid (black solid curve) (Fig. 12c), NHW 500-m resolution grid with 3 σ -layers (red solid curve) (Fig. 12d), NHW 250-m resolution grid with 3 σ -layers (red short dash curve) (Fig. 9c), and NHW 500-m resolution grid with 5 σ -layers (red long and short dash curve) (Fig. 9d)

because of the better resolved bathymetry). Figure 10b shows that increasing the number of σ -layers from 3 to 5, thereby doubling the vertical grid resolution, yields slightly faster waves of similar surface elevation nearshore (although there appears to be slightly larger differences in elevation offshore). Finally, Fig. 11 shows envelopes of maximum surface elevations computed along the same transect, for the various cases discussed before. Although there are larger differences over the continental shelf slope, as a function of discretization resolution and number of σ -layers, nearshore, all the computed maximum elevations are in good agreement, which supports our choice of model parameters for NHW.

3.4.3 Coupling of NHW and FNW to simulate the tsunami coastal propagation

We verify the relevance and accuracy of the one-way coupling of NHW's 3D results, obtained in a 500-m resolution grid with 3 σ -layers, to FNW's 2D results in a horizontal grid with identical 500-m resolution and surface area, to pursue simulations of nearshore propagation and coastal impact. Based on the tsunamigenic duration of slide motion (Fig. 6), FNW is initialized with NHW results soon after the end of slump motion, i.e., at $t = 800$ s (13.3 min; Fig. 7d). Because the horizontal grids have identical cells in both models, surface elevation and horizontal velocity (interpolated at the required level of 0.513 times the local depth, from σ -layer results in NHW) are easily used to initialize FNW and pursue computations in this model for later times. To prevent reflection at open boundaries, sponge layers are specified in FNW's grid over a width of 60 km or 120 grid cells inward from the northern and southern boundaries, and 100 km or 200 grid cells inward from the eastern boundary (see details in Shi et al. 2012). These sponge layers do not fall within the zoomed-in area used to visualize results.

In Fig. 12, we compare both instantaneous and maximum surface elevations computed in NHW at $t = 33$ min to FNW's results computed at the same time, after being initialized with NHW results at 13.3 min (Note, because no bottom friction was specified in NHW during these simulations, for the purpose of comparison, these FNW simulations also assume a bottom friction coefficient $C_d = 0$. Because the tsunami is still in fairly deep water, however, this should not matter for results computed at this stage of propagation).

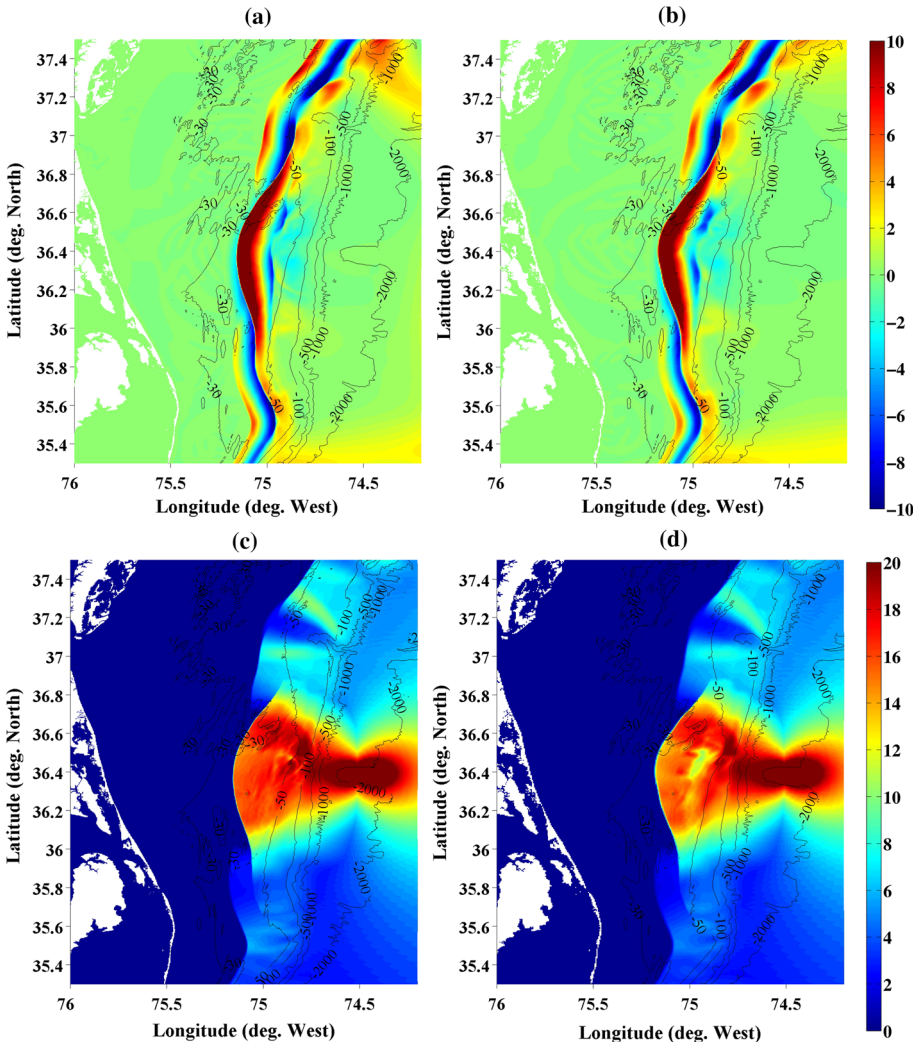


Fig. 12 Instantaneous (a, b) and maximum (c, d) surface elevations (*color scale* is in meter) in simulations of the Currituck SMF tsunamis, at $t = 2,000$ s (33.3 min) after SMF triggering, computed using ($C_d = 0$; 500 m horizontal grid): (a, c) FNW; (b, d): NHW (with 3 σ -layers). FNW is initialized from NHW results computed at 800 s (13.3 min; Fig. 7). Results are shown in zoomed-in area of Fig. 2; bathymetric contours are marked in meter

We see that results of both models are in good agreement at this stage. The same surface elevations are compared in Fig. 10c, at various times, and in Fig. 11 for the maximum envelope along an E-W transect passing through the SMF center. Again, FNW and NHW results obtained on the same horizontal grid are in good agreement nearshore, over the continental shelf. In the transects of Fig. 10c, surface elevations computed over the shelf in both models appear to be nearly identical, with FNW's results only slightly lagging in time as compared to NHW's results. Such a time lag, however, does not affect maximum inundation and runup.

Figure 11 confirms these observations. In shallow water, for $x \leq -25$ km (or depth < 45 m), the maximum envelopes of surface elevation computed at 33 min with FNW and NHW (using 3 σ -layers) are in good agreement. From $x = -15$ to -25 km, discrepancies are larger, but this is likely due to small “numerical adjustments” of NHW’s initial solution to the parameters and grid used in FNW. Finally, for $x = -25$ to -35 km, differences of NHW’s solution using 5 σ -layers with other solutions are larger, likely due to the more complex velocity profile over depth in this larger depths area, which is better represented with 5 layers. In shallower water, however, the 5-layer solutions are in good agreement with the 3-layer solution.

The good agreement between FNW and NHW results for maximum surface elevation and wave profiles in shallow water thus supports using the two model coupling approach that will be used in all the following simulations in this work.

3.5 Simulation of the Currituck SMF tsunami propagation to shore

3.5.1 Coarse grid regional and nearshore simulations

We compute the Currituck tsunami propagation to shore with FNW, by one-way coupling in a series of nested Cartesian grids. Simulations start in the 500-m resolution regional grid used so far for the convergence and accuracy study, still initialized at 800 s with NHW results, but computations are run for a longer time than before. We use the standard value of the bottom friction coefficient, $C_d = 0.0025$, corresponding to coarse to fine sand. In their simulations along a one-dimensional cross-shore transect, Geist et al. (2009) studied the sensitivity of SMF tsunami elevation to bottom friction and showed that using larger friction coefficient values significantly reduced tsunami coastal impact. We tested this as well in our simulations (results not shown) and observed that for $C_d = 0.01$ the inundation depth along the shore near Virginia Beach is reduced by a factor of 2 or more, as compared to simulations using $C_d = 0.0025$. Hence, such large values should not be used for tsunami hazard assessment, unless they can be clearly justified by land use and/or the anticipated amount and size of coastal debris transported by the tsunami flow. This important aspect of modeling tsunami coastal impact will be left out for future work.

Figure 13 shows a sequence of instantaneous surface elevations computed with FNW in the 500-m resolution grid, up to $t = 99$ min, at which time tsunami waves are impacting the entire coastline from North Carolina to Virginia Beach (Fig. 1). As a result of frequency dispersion, the tsunami wave train that propagates toward shore is made up of a series of elevation and depression waves. Specifically, between 82 and 99 min, the leading tsunami waves reach the entire shoreline of the barrier islands south of Virginia beach, down to the outer banks of North Carolina, causing 5–6 m maximum surface elevations that overtop the barrier island at many locations (Fig. 13c, d). At 99 min, 2–3 m elevation waves also reach the south of the Delmarva peninsula eastern shore and the mouth of the Chesapeake Bay (Fig. 13d). Clearly, however, the 500-m resolution grid used here is insufficient to accurately compute nearshore propagation and coastal tsunami impact (inundation and runup). This is done below in smaller nested grids, with 125- and 32-m resolution.

Figure 14a shows the envelope of maximum surface elevation computed in the 500-m FNW grid up to 99 min (same results as in Fig. 13). As expected for a SMF tsunami (e.g., Tappin et al. 2008), we observe a fairly narrow directional spreading of the largest waves, both onshore and offshore. We also see a fairly large decrease in maximum surface elevation westward, toward shore. This decay is further illustrated in Fig. 14b, along an

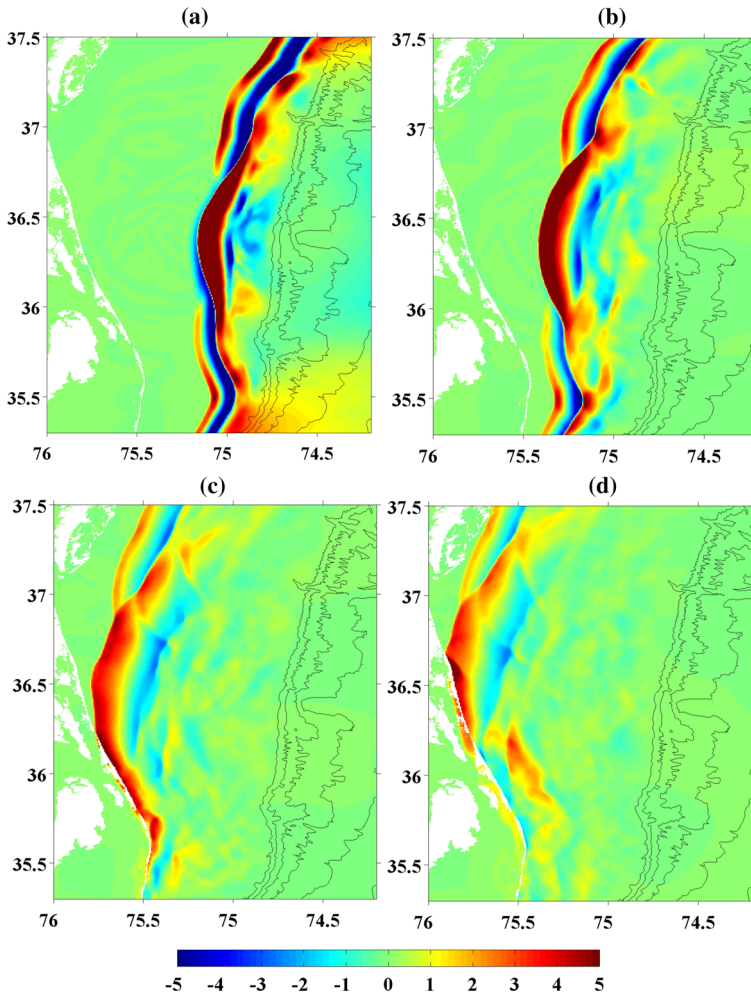


Fig. 13 Instantaneous surface elevation (*color scale* is in meters) in FNW simulations of the Currituck SMF tsunami ($C_d = 0.0025$; 500 m resolution grid), initialized from NHW results at 800 s ($C_d = 0$; 500-m resolution grid; 3 σ -layers; Fig. 7), at $t =$ (a) 33; (b) 49; (c) 82; and (d) 99 min. Results are shown in zoomed-in area of Fig. 2; axes are lat ($^{\circ}$. N) and lon ($^{\circ}$. W)

E-W transect, and is due in part to directional spreading of wave energy and in part to dissipation from bottom friction over the wide and shallow shelf and, in shallower water, wave breaking closer to shore. Although Geist et al.'s (2009) Currituck source parameters, method of tsunami generation, and grid resolution differ from ours in a number of important aspects, numerical results in their Fig. 4 can be compared to those in Fig. 13, which show surface elevations computed at similar times; Fig. 14 can also be similarly compared to Geist et al.'s (2009) Fig. 5a, b. Overall, we find a good qualitative agreement between both studies, but our results show more complex wave trains that also seem to be more influenced by the bottom bathymetry, perhaps in part because of the higher resolution of our simulations (better seen in the next section). We also predict a longer characteristic

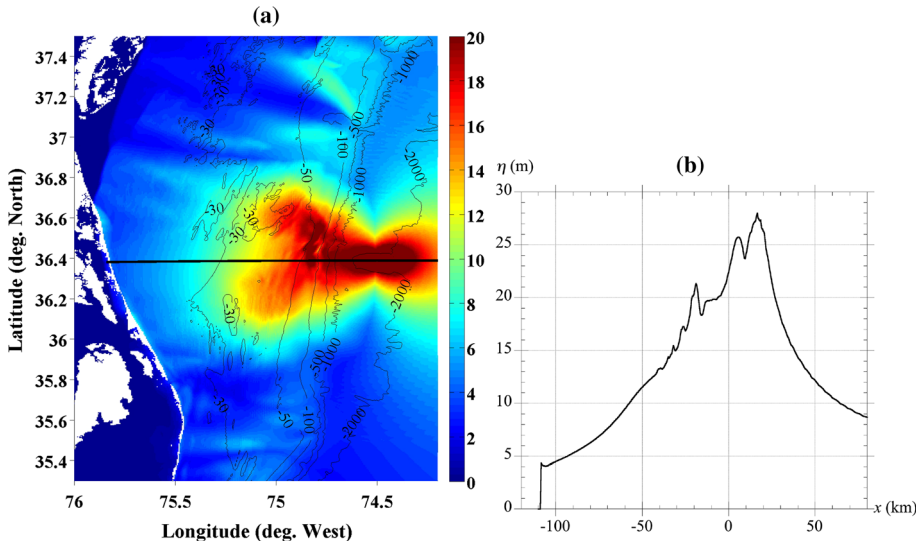


Fig. 14 Maximum surface elevation in FNW simulations of the Currituck SMF tsunami, up to $t = 99$ min ($C_d = 0.0025$; 500 m resolution grid): **a** over the entire 500-m resolution grid (elevation color scale in meter and bathymetric contours in meter); **b** along an E-W transect (marked by the *black solid line* in **a**) through the SMF center, in the direction of the Currituck Banks, as a function of the distance to the SMF center

wavelength of incoming waves than in Geist et al. and a slightly larger leading wave, relative to the rest of the incoming wave field. This longer wavelength and other differences in the generated incoming wave train result from differences in pre-failed SMF reconstruction, wave generation modeling (ours being 3D while theirs is 2D), and model type and resolution, between the present work and Geist et al.’s. While maximum predicted surface elevations are in reasonable agreement nearshore, we also note that the spread of the surface envelope is wider in the present FNW results than in Geist et al.’s study.

Finally, Geist et al. (2009) also pointed out that outgoing (i.e., offshore propagating) waves generated by the Currituck SMF, although initially propagating toward a dominant eastward direction, ended up refracting on the northern part of the shelf, causing a large impact along the coast of New Jersey (see their Fig. 11). We verified that this also occurred in our simulations, by using a larger 800 by 800 km, 1,600 by 1,600 mesh FNW grid, with identical 500-m resolution ($C_d = 0.0025$; SW corner at 32.72N 79.18W; 100-km-thick sponge layers on the eastern boundary and 60 km on the southern and northern boundaries). Simulations are again initialized from NHW results at $t = 13.3$ min (with 3 σ -layers; $C_d = 0$). Figure 15 shows the instantaneous surface elevations computed at 55 min, at which time some of the smaller waves that were initially propagating offshore in the smaller domain (e.g., Fig. 7d; northern part of the outgoing cylindrical wave) have been bent to the north by refraction into propagating onshore, over the continental shelf slope and shelf. For the NTHMP tsunami inundation mapping work, this indicates that simulations in nested grids of the four SMF sources (Fig. 1) should be initiated in a large enough domain (even larger than used in Fig. 15), to accurately capture such wave refraction effects.

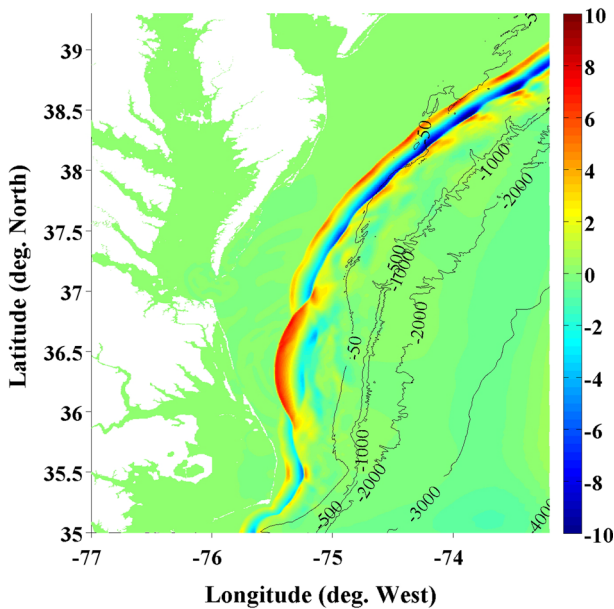


Fig. 15 The same FNW computations as in Fig. 13, but over a larger 500-m resolution grid (800 by 800 km; 1,600 by 1,600 grid; $C_d = 0.0025$; SW corner at 32.72N 79.18W), in order to better simulate wave refraction over the northern continental slope off of New Jersey

3.5.2 Fine grid nearshore simulations off of Virginia Beach and in the Chesapeake Bay

Using FNW in finer resolution nested grids, we compute in greater detail the impact caused by the Currituck SMF tsunami on the nearest most affected coastal areas around Virginia Beach (36.8N) and the mouth of the Chesapeake Bay (37N). Besides the interest of better assessing coastal tsunami impact than in the coarser regional grid, these simulations will validate the one-way coupled computations in nested grids, which will also be used for tsunami hazard assessment along the entire USEC. The reference level in these simulations is the so-called sea level, defined by NOAA-NGDC as approximately the Mean Low Low tide (MLLT) level. By contrast, in the SMF tsunami hazard assessment, we will perform for the USEC, using the four SMF proxies; the reference level in the finer coastal grids will be increased to mean high water (MHW) level.

Simulations are performed with FNW in 125- and 32-m resolution nested grids, located on the shelf, west of the source area (Fig. 16). Due to the fairly narrow incident wave train at this stage, simulations in the 125-m resolution grid are initialized (for this case only) by interpolating FNW 500-m resolution grid results (surface elevation and current), once salient waves have completely entered the finer grid; simulations in the next level of nesting (32-m resolution grid) will then be pursued by one-way coupling. Initialization was deemed acceptable at $t = 26.6$ min, which is the time of the instantaneous surface elevation shown in Fig. 16 (as computed in the 500-m resolution grid). Simulations in the 32-m resolution grid will be forced along the boundary, from time series computed in the 125-m resolution grid results, also starting at $t = 26.6$ min.

More specifically, Fig. 16 shows the footprint of the 500-m FNW regional grid (900 × 800 mesh; 450 by 400 km; see also Fig. 2). The 125-m resolution grid is defined

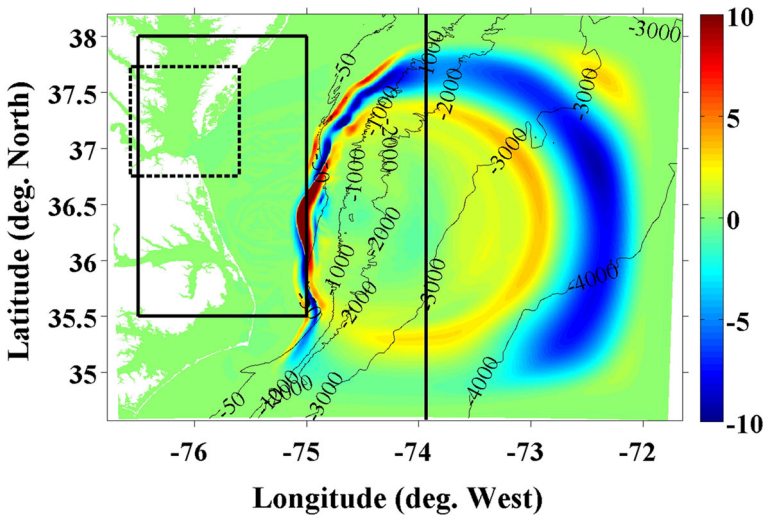


Fig. 16 Free surface elevation (*color scale* is in meters) at $t = 26.6$ min in FNW simulations of the Currituck SMF tsunami (in 450×400 km area, 500-m resolution grid; $C_d = 0.0025$; initialized at 13.3 min from NHW 500-m resolution grid results). At this time, simulations are initialized in the 125 m (to the left of the black line at 73.9W) and restarted in the 32 m (dashed black box), resolution grids. The black box is the zoomed-in area used to show results in Figs. 17 and 19. Bathymetric contours are marked in meter

on the west side of this grid (marked by a vertical solid line in the Fig. ($1,997 \times 3,197$ mesh; 160 by 400 km; SW corner located at 76.8W and 34.6N, as for the 500 m resolution grid). The footprint of the 32-m resolution grid is marked by the smaller dashed box located within the 125-m resolution grid ($3,565 \times 2,913$ mesh; 111.4 by 91 km; SW corner located at 76.57W and 36.75N). Sponge layers in the 125-m resolution grid are 60 km thick on the eastern boundary and 50 km thick on the northern and southern boundaries. Results will show that the northern and southern tsunami wave tails are properly damped in the sponge layers, while the main westward propagating tsunami waves, which dominate hazard for Virginia Beach and the Chesapeake Bay, are not affected. No sponge layers are needed in the 32-m resolution grid since both incident and reflected waves are included in the time series used as boundary conditions, which hence satisfies the offshore open boundary conditions. Computations in the 125- and 32-m resolution grids are run from $t = 26.6$ –250 min, to make sure that wave reflection off the various coastal boundaries is accounted for in the time series used in the 32-m resolution grid, thus fully satisfying the open boundary conditions. This approach was successfully used to simulate the Tohoku 2011 tsunami with three levels of nesting (Grilli et al. 2013b).

Results of simulations in the 125- and 32-m resolution grids are shown in Figs. 17, 18, 19, 20. The black box in Fig. 16 (76.5–75W and 35.5–38N) marks the zoomed-in area used in Figs. 17 and 19 to show 125-m resolution grid results, centered around Virginia Beach and the mouth of the Chesapeake Bay.

Figure 17 shows a time sequence of instantaneous free-surface elevation, computed from $t = 26.6$ –200.6 min in the 125-m resolution grid. Over this time, the tsunami propagates both westward toward the North Carolina and Virginia Beach coastlines as well as northwestward into the Chesapeake Bay. We note that Fig. 17b approximately corresponds to the surface elevation hazard computed in the 500-m resolution grid shown in Fig. 13c.

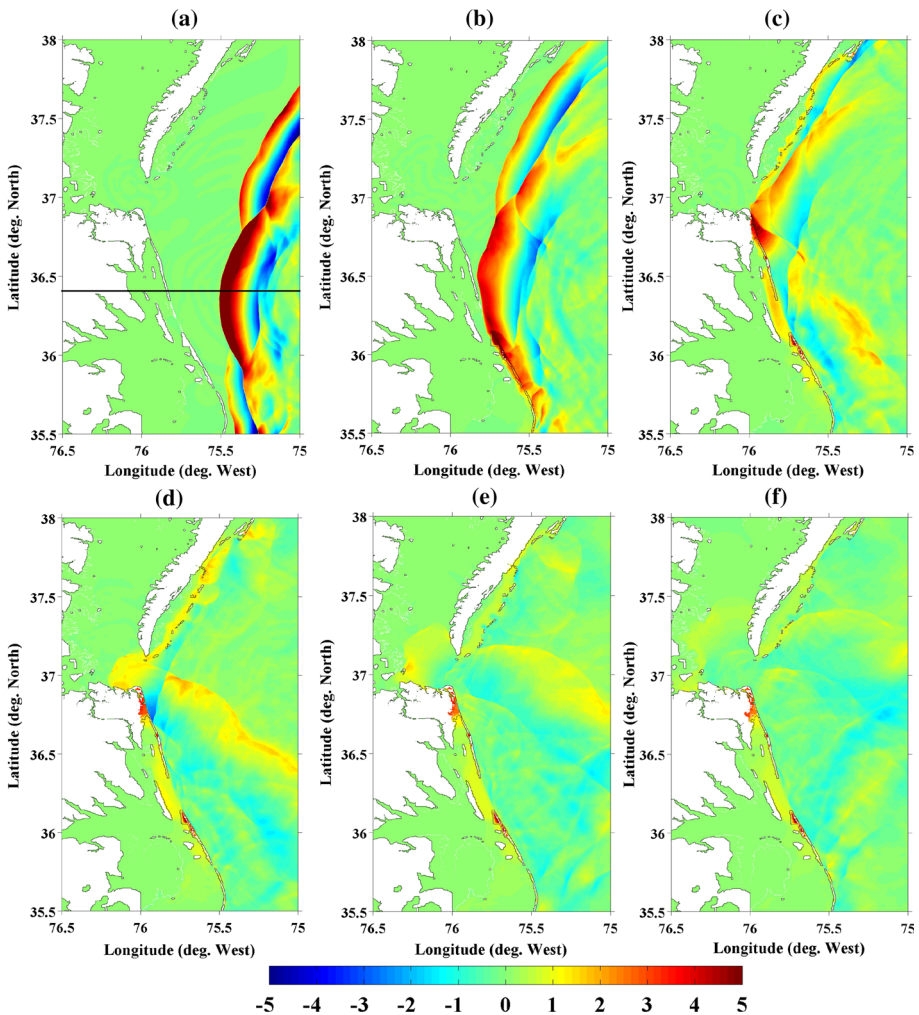


Fig. 17 Instantaneous surface elevation (*color scale* in meters) in FNW simulations of the Currituck SMF tsunami in the 125-m resolution grid ($C_d = 0.0025$) (Fig. 16), initialized at 26.6 min from FNW 500-m resolution grid results. Results are shown over the zoomed-in area marked in Fig. 16, at $t =$ (a) 56.6; (b) 86.6; (c) 116.6; (d) 146.6; (e) 176.6; and (f) 200.6 min. The *black solid line* in panel (a) marks the E-W transect in the direction of Currituck Banks, where results are shown in Fig. 18

Clearly, wave patterns and surface elevations appear to be very similar, although, as expected, more details can be seen in the 125-m resolution grid results. The good agreement between 125- and 500-m resolution grid results is further confirmed in Fig. 18, which compares surface elevation computed along an E-W transect through the SMF center (marked in Fig. 17a).

Differences between 125- and 500-m resolution grid results, as could be expected (Grilli et al. 2013a), are mostly: (1) a steeper front of the leading wave and (2) higher-frequency oscillations in the trailing oscillatory tail of the tsunami wave train. Note that profiles (b, d, f) shown along the transect correspond to the times of Fig. 17a, b, c, respectively.

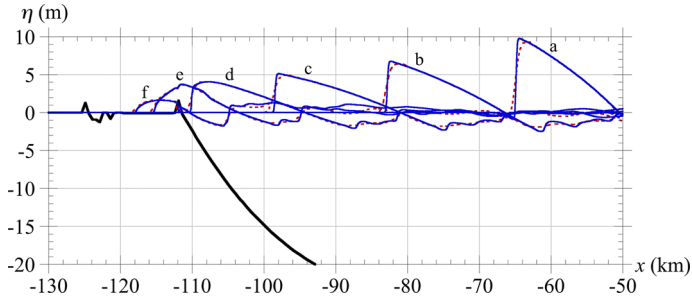


Fig. 18 Comparison of instantaneous surface elevations in FNW simulations of the Currituck SMF tsunami ($C_d = 0.0025$) along an E-W transect through the SMF center (36.39N lat.; Fig. 17a), as a function of the distance to the center of the SMF, in 125 m (solid curve) and 500 m (short dash curve) grids. Computations are initialized in the 500-m resolution grid from NHW 500-m resolution grid results at 13.3 min, and in the 125-m resolution grid from 500-m FNW resolution grid results at 26.6 min. Surface profiles are shown at $t =$ (a) 41.6; (b) 56.6; (c) 71.6; (d) 86.6; (e) 101.6; and (f) 116.6 min; (thick solid curve) denotes the ocean depth

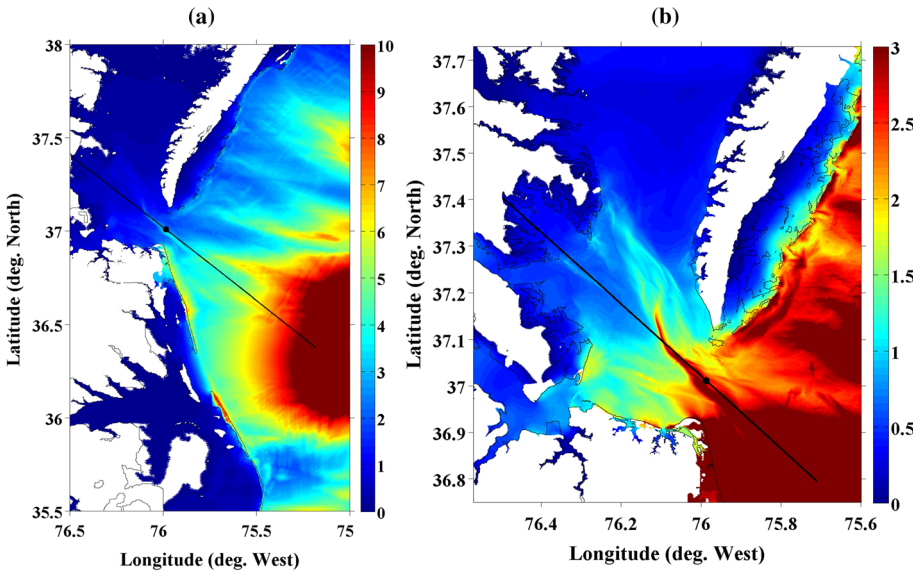


Fig. 19 Maximum surface elevation (color scale is in meters) up to $t = 250$ min, in FNW simulations of the Currituck SMF tsunami ($C_d = 0.0025$): a in the 125-m resolution grid (Figs. 16, 17; results are shown over the zoomed-in area marked in Fig. 16); b in the 32-m resolution grid (Fig. 16). The black lines mark the location of a transect used for showing surface elevation in Fig. 20 ($x = 0$ is marked by a black dot). The zero-elevation shoreline is marked as a black contour level in both figures, showing the extent of flooding

Regarding coastal tsunami impact, toward the end of simulations in Figs. 17 and 18, the entire barrier island from Virginia Beach to the south of it is overtopped by waves of over 5 m elevation; maximum tsunami impact occurs in Virginia Beach at $t = 116$ min (Fig. 17c). For later times, the tsunami floods inland areas around Virginia Beach and further south, while large waves also propagate into the Chesapeake Bay. In particular, refraction north of Virginia Beach causes waves to be diverted around the headland and

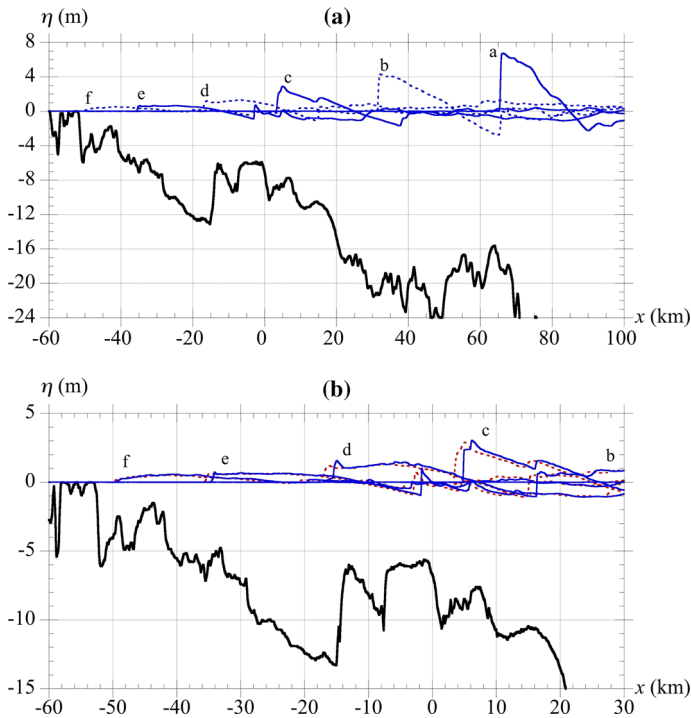


Fig. 20 Instantaneous surface elevation in FNW simulations of the Currituck SMF tsunami ($C_d = 0.0025$), along the transect marked in Fig. 19 ($x = 0$ at the mouth of the Chesapeake Bay): **a** in the 125-m resolution grid (solid curve, short dash curve); and **b** in the 32 m (solid curve) and 125-m (short dash curve) resolution grids (Fig. 16). Surface profiles are shown at times: $t =$ (a) 56.6; (b) 86.6; (c) 116.6; (d) 146.6; (e) 176.6; and (f) 200.6 min

impact the Norfolk area with 2–3 m surface elevations (Fig. 17d). This can also be seen in the maximum surface elevations shown in Fig. 19, where the Virginia Beach-Norfolk area is flooded with 3–6 m inundation. Maximum surface elevations at the mouth of the Chesapeake Bay are about 3 m. The 125-m resolution grid resolution, however, is not sufficient to properly resolve both small-scale coastal morphology features and shorter higher-frequency waves that would be generated near the front of leading tsunami wave crests (i.e., dispersive shock waves; see Geist et al. 2009, Fig. 12 and Grilli et al. 2013a; Fig. 10). This would require grid resolutions of 10 m or less and will be the object of future work, planned in the Virginia Beach-Norfolk area as part of NTHMP.

Tsunami propagation into the Chesapeake Bay is nevertheless further analyzed here in the finer 32-m resolution grid. Figure 19 compares maximum surface elevations computed in the 125- and 32-m resolution grids and, in particular for the latter, shows the significant extent of inundated areas, both along the ocean exposed shores and inside the Bay (compare maximum penetration of the inundation to the zero-level shoreline shown as a black contour), although surface elevations appear to rapidly decrease as the tsunami propagates into the Bay. In this respect, Fig. 20 compares surface elevations computed in both 125- and 32-m grids along a transect into the Bay (marked in Fig. 19), for the same time sequence as in Fig. 17. While the tsunami elevations reach nearly 7 m over the shelf, they reduce to 3 m at the mouth of the Bay ($x = 0$ here) and then to 1 m further inside the

fairly shallow Bay. Figure 20b compares results computed in the 125- and 32-m resolution grids for 5 times; while there are shorter wavelength waves resolved in the 32-m resolution grid results, surface elevations are essentially identical, although there is a space/time lag between both grid results. Because of the shallowness and complex bathymetry of the Bay, results in the 32-m resolution grid are expected to be more accurate, particularly, for predicting details of maximum inundation along the complex shoreline, as also seen in Fig. 19b.

4 Simulation of SMF tsunami hazard along upper USEC for NTHMP

4.1 SMF source selection and sediment availability in study area

As discussed in the introduction, as part of tsunami inundation mapping work done for NTHMP, SMF tsunami hazard is assessed along the upper USEC using SMF proxies similar to the historical Currituck slide (Fig. 2). These tsunamis represent worst-case scenarios equivalent to the probable maximum SMF tsunami in the region from Virginia to Cape Cod. These SMFs were sited on the basis of: (1) earlier geotechnical work and slope stability analyses based on Monte Carlo simulations (MCS; Grilli et al. 2009; Krauss 2011) and (2) actual field data on sediment and sub-bottom profiles (Eggeling 2012). This led to selecting four areas, marked in Fig. 1 as Study Areas 1–4, which have a clear potential for large tsunamigenic SMF sources, both in terms of low slope stability safety factors and sufficient sediment availability for causing large SMFs. Among those, Grilli et al.'s (2009) MCS results (their Fig. 18) indicated that Areas 3 and 4, which are located off of Atlantic City, NJ, have the highest potential for tsunamigenic SMFs. In addition to this area, MCS results also identified an increased tsunami risk off of the Hudson River estuary and the Long Island southern coastline, which correspond to SMFs occurring approximately within Study Areas 1 and 2.

More specifically, Eggeling's (2012) analysis of sediment availability in the four study areas concluded that Area 1, in the Hudson Apron (Figs. 1, 21a), is characterized by large soil deposits, because it has experienced high sedimentation rates during the Pleistocene. Since most landslides along the US Atlantic continental margin consist primarily of Quaternary sediment (a combination of Pleistocene and Holocene sediment), this site likely contains enough sediment for a Currituck volume SMF to occur. In Area 2, which is located southwest of Ryan Canyon (Figs. 1, 21b), Eggeling (2012) reported that, on the basis of a cross-slope survey, there is sufficient sediment available to cause a 20-km-wide SMF; hence, this area likely also has both appropriate and thick enough sediment for a Currituck SMF proxy to occur. In Areas 3 and 4 (Figs. 1, 21c, d), which are located in the Baltimore Canyon, results of deep drilling from the USGS indicate that there is a substantial thickness of Quaternary sediment (J. Chaytor, personal communication, 2013, USGS). However, in some locations, sediment thickness does not exceed ~100 m, as can be seen in cross-slope transects made through these areas, which show several hills 3–5 km wide, with a vertical distance between peaks and valleys of roughly 200–400 m (Fig. 23). Assessing whether the amount of sediment available is sufficient for a Currituck size SMF is difficult at these two locations, as the continuous action of downslope processes along the mid and north US Atlantic margins leads to variable along slope thicknesses on a ridge to ridge scale (J. Chaytor, personal communication, 2013, USGS). Despite these uncertainties, and consistent with the PMT approach adopted in this NTHMP work, we assumed that a failure of volume sufficient for a Currituck SMF proxy could extend slightly deeper

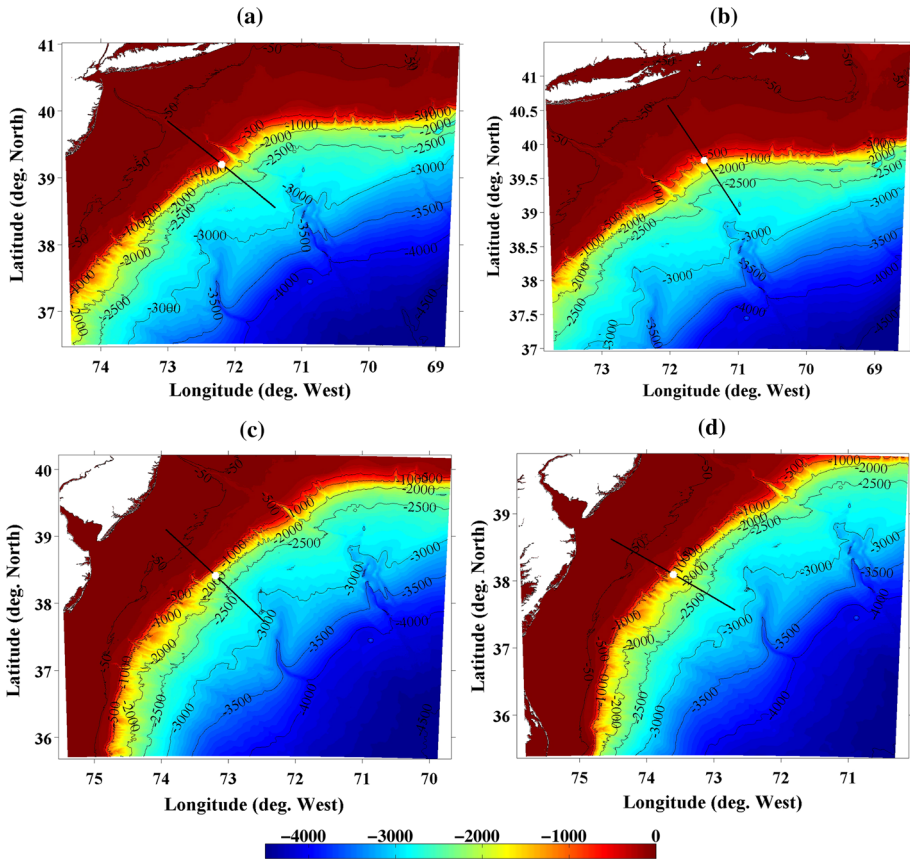


Fig. 21 Bathymetry (color scales and contours in meter) in Study Areas (Fig. 1): **a** 1; **b** 2; **c** 3; and **d** 4; (solid curve) mark locations of transects in SMF direction of motion θ , through SMF centers, shown in Fig. 22, and white dots mark the initial center of mass initial (x_0, y_0) of each SMF proxy (Table 1)

than the available sediment accumulation in these study areas, thus representing multiple ridges failing at once.

4.2 Simulation of tsunami sources for Currituck SMF proxies in study Areas 1–4

Figure 21a–d shows the bathymetry near and around study Areas 1–4, in which Currituck SMF proxies were sited to assess tsunami hazard along the upper USEC (Note that several small spurious steps in the bathymetry were observed, which were removed using a filtering function prior to performing tsunami simulations). The white dots in the figures mark the four SMF proxy initial center of mass locations (x_0, y_0) , and the black lines are transects through each center, in the selected azimuthal direction of SMF motion θ ; for each site, both of these were inferred from seafloor morphology. Specific parameters for each SMF, which all correspond to Currituck proxies of same length, width, and thickness, as well as information on numerical grids used in NHW simulations are listed in Table 1.

More specifically, in light of the historical Currituck event detailed before, the location (x_0, y_0) of each SMF proxy was selected in their respective area as a function of local

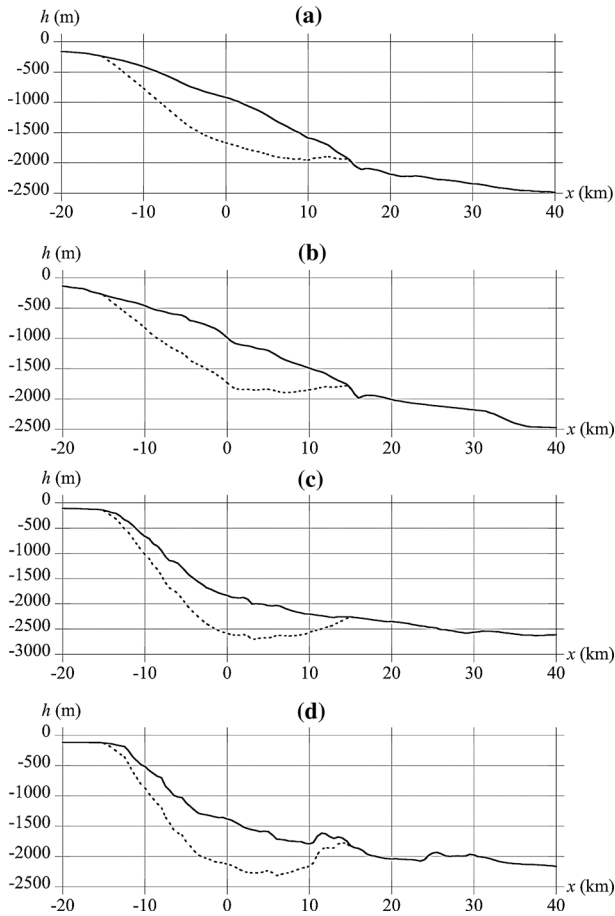


Fig. 22 Transects through SMF proxy centers (x_0, y_0) in azimuthal direction θ (Table 1) in Study Areas (Figs. 1, 21): **a** 1; **b** 2; **c** 3; and **d** 4; (solid curve) current bathymetry; (short dash curve) cross-section of a Currituck SMF proxy (at time $t = 0$ in simulations)

seafloor morphology to replicate the headwall of Currituck Slide 2 (Locat et al. 2009), where $\sim 150\text{--}200$ m of sediment was removed by the landslide at the 500-m post-exca- vation depth location. Based on these, the assumed direction of motion θ and Quasi- Gaussian shape of each SMF [Fig. 3 and Eqs. (1–2)], their initial bathymetry was con- structed for each site. The resulting main SMF cross-sections along each transect marked in Fig. 21a–d are shown in Fig. 22a–d; in the latter figures, we see that despite having the same overall dimensions, each SMF, once place in its site-specific location, has quite a different cross-section.

Owing to the similarity of the bathymetric gradient in all selected areas (see depth contours in, e.g., Fig. 1), an identical average slope of $\alpha = 4^\circ$. was used as the repre- sentative continental shelf slope for each site, to be used in Eq. (4). For each SMF, the kinematics $s(t)$ is computed by Eqs. (3–7), using parameters listed in Table 1. Since all the parameters governing each SMF proxy’s motion are identical, runout and total time of

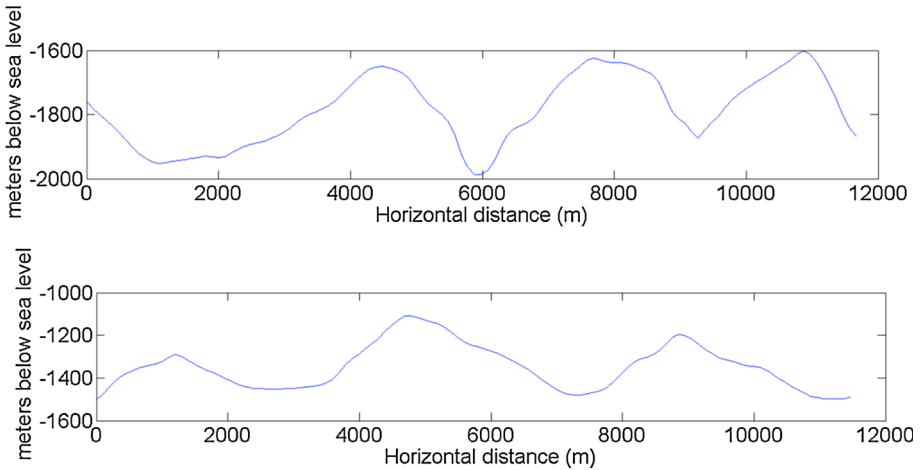


Fig. 23 Cross-slope bathymetric transects in Areas 3 (*top*) and 4 (*bottom*) (Figs. 1, 21c, d), from Eggeing (2012)

motion are also identical for the 4 SMFs, i.e., $s_f = 15.8$ km and $t_f = 710$ s (Table 1). Based on these values, NHW (3 σ -layers; $C_d = 0$) was run to compute each SMF tsunami source, for 13.3 min (800 s) in four separate 500-m resolution grids whose footprints are marked in Fig. 24 (Table 1), yielding the simulated surface elevations shown in Fig. 24a–d. The figure shows that the initial features of each tsunami source are qualitatively identical, although, as expected, there are differences in surface elevation and dominant direction of wave propagation, due to site-specific effects of bathymetry on wave generation and propagation.

NHW results are then used to initialize many additional simulations of tsunami propagation with FNW ($C_d = 0.0025$), in a series of finer nested coastal grids, in order to compute tsunami inundation maps along the USEC. These FNW simulations all start in the 500-m Cartesian grid shown in Fig. 25 (upper left panel), where each SMF tsunami source is specified one at a time, but then the next level of nesting, in 122-m resolution grids, is different for each sector of the upper USEC, each corresponding to a high-resolution NOAA-NGDC DEM (see red boxes in Fig. 25, upper left panel). Full simulations have been completed to date for six such sectors/DEMs, of which due to lack of space we only provide detailed results in the next section, as an illustration, for the very exposed Ocean City, MD area. The final high-resolution inundation maps for the entire upper USEC will be posted on NOAA-NTHMP's Web site at the completion of this project.

4.3 Detailed modeling of SMF tsunami inundation mapping in Ocean City, MD area

As discussed in the introduction, as part of the NTHMP inundation mapping activity along the USEC, both far-field and near-field SMF tsunami sources are considered, but only the work dealing with SMF tsunami hazard is reported here.

Thus, in the following, we detail simulations performed with FNW for the Ocean City, MD sector/DEM, to develop high-resolution inundation maps resulting from the impact of the four SMF tsunami sources computed above (Fig. 24). To do so, we first define a series of nested Cartesian grids, from an initial 500-m grid in which SMF sources are specified

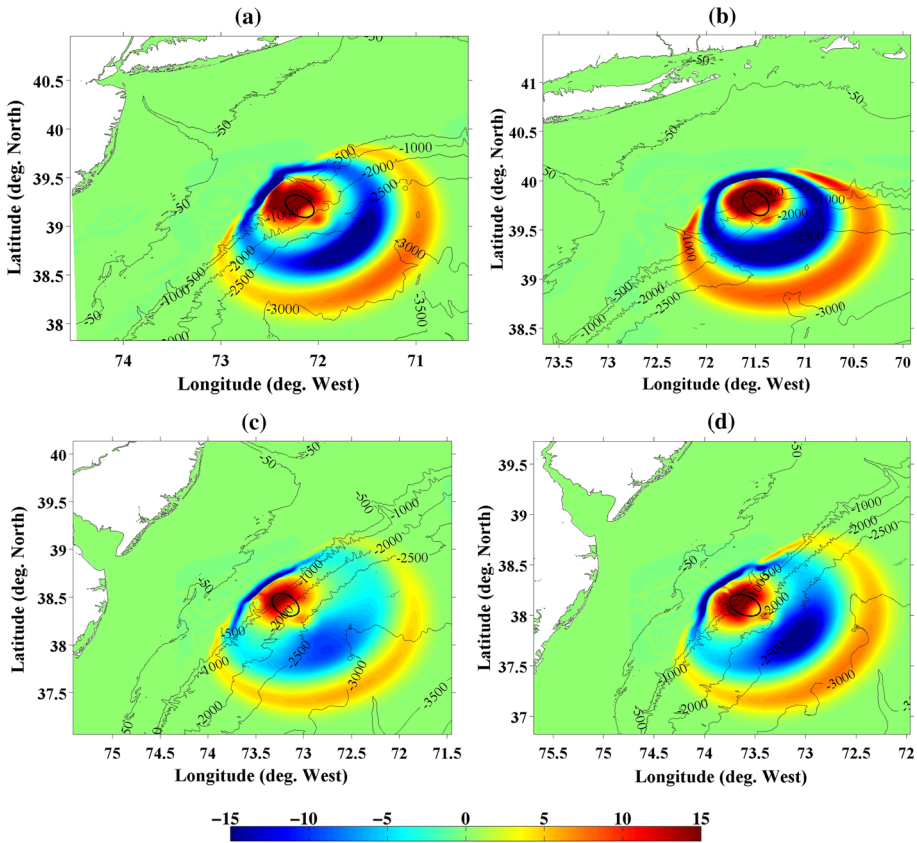


Fig. 24 Surface elevation (*color scale* in meter) of tsunami sources, for four SMF proxies whose initial footprint is marked by a *black ellipse*, simulated with NHW (500-m resolution grids with 3 σ -layers, $C_d = 0$) in four selected areas (Figs. 1, Fig. 21): **a** 1; **b** 2; **c** 3; and **d** 4. Results are shown at 13.3 min after SMF triggering (after the SMFs have stopped moving). SMF sources in areas 1–4 are parameterized as Currituck proxies (Fig. 22 and parameters in Table 1). Bathymetric contours are marked in *meters*

down to many high-resolution 10-m grids, in which inundation depth and other products are computed (Fig. 25); to ensure good accuracy and stability of these one-way coupled simulations, the ratio of grid mesh size between two successive nesting levels is limited to around 4. To define bathymetry/topography in each nested grid, for each particular resolution, we use commensurately accurate data interpolated from: (1) ETOPO-1 1 arc-min and NOAA-CRM 3 arc-sec data in deeper water and over the shelf and (2) nearshore, from NOAA-NGDC Ocean City 1/3 arc-sec DEM (Grothe et al. 2010). As shown in Fig. 25, this DEM covers a major area of the Delmarva Peninsula, from the southern part of Delaware Bay down to Metompkin Bay in Virginia. The DEM datum for these simulations is set to mean high water (MHW).

The nested FNW Cartesian grids are all shown in Fig. 25, i.e.: (1) a $1,500 \times 1,500$ mesh, 500-m resolution grid, in which the four SMF proxy sources of Fig. 24 (marked by green dots in the upper left panel) are specified as initial conditions (one at a time); (2) the “Ocean City DEM” grid, a $627 \times 1,072$ mesh, 122-m resolution

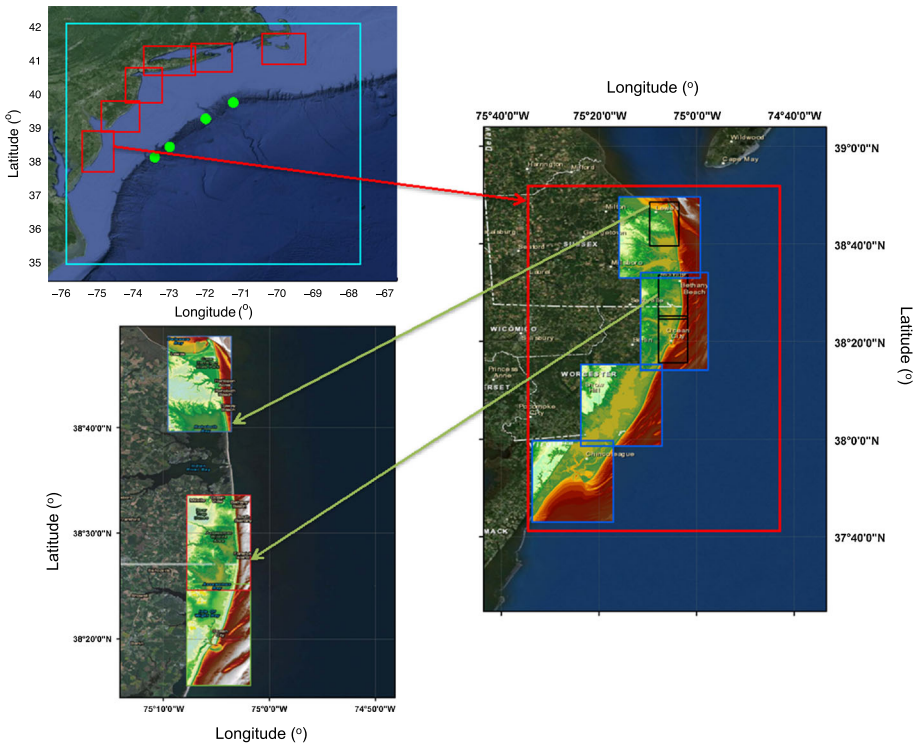


Fig. 25 FNW nested grids used for detailed inundation mapping along the upper USEC, with details of the Ocean City, MD area. *Upper left panel:* (blue box) 500-m resolution grid initialized by the four SMF proxy sources of Fig. 24 (marked by green dots); (red boxes) boundary of 122-m resolution grids for each sector/DEM used so far along USEC, with the lowest being the Ocean City DEM. *Right panel:* (red box) Enlarged area of 122 m Ocean City grid; (blue boxes) 30-m resolution grids OC-1 to OC-4; and (black boxes) finer 10-m resolution grids defined in areas of greatest interest or impact. *Lower left panel:* enlarged areas of two 10-m grids (lower: Bethany Beach area; upper: Lewes area)

nested grid (red box in right panel); (3) Grids OC-1 to OC-4, $750 \times 1,000$ mesh, 31-m resolution grids (right panel); and (4) a few finer $1,080 \times 1,620$ mesh, 10-m resolution grids defined in areas of greatest interest or impact. Only the 500-m grid has sponge layers, and the 122- and 31-m grids are used in one-way coupling simulations.

Simulations of the four SMF proxies in the 500-m grid (not detailed here) indicate that the SMF sited in Area 4, which is the closest to Ocean City, causes maximum impact in the 122-m grid. Hence, only this SMF was used in subsequent inundation mapping for this sector/DEM; note that other SMFs will be dominant in different DEM sectors (not detailed here). Simulations of tsunami propagation are pursued by one-way coupling in the 122-m grid (also not detailed here), using time series of surface elevation and depth-averaged current computed in the 500 m grid, as forcing along its ocean exposed boundary (Fig. 24, Fig. 25), and then in the four 31 m resolution nested grids OC-1 to OC-4, for which inundation results are shown in Fig. 26; in the latter figures, we see that significant areas along the shore would be impacted by over 2-m-deep inundation.

One final level of nested simulations is performed in the 10-m grids (Fig. 25), for some of the most impacted or critical areas. In these highly resolved simulations, besides

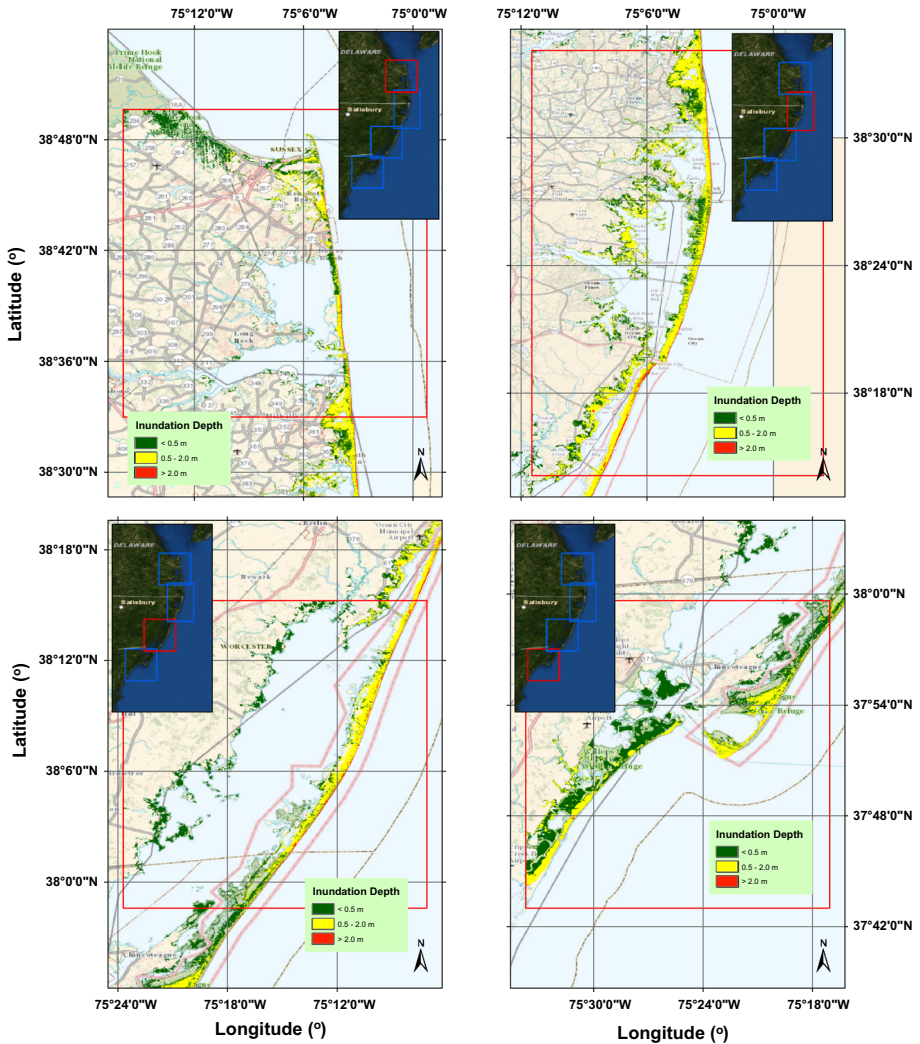


Fig. 26 Maps of tsunami inundation depth computed with FNW in 31-m resolution Grids OC-1 to OC-4 (see Fig. 25 and insets for actual locations); one-way coupled simulations are forced on their boundary by time series of surface elevation and currents computed in the 122 m Ocean City grid, for the area 4 SMF proxy (Fig. 24)

inundation depth and penetration, we computed other metrics that can be helpful in quantifying tsunami impact, depending on the type of land use or coastal structures that are considered. Figure 27 thus shows a map of the tsunami-induced maximum momentum flux ($N \times m$) in the highly developed area of Bethany Beach, DE (Fig. 25). This metric can be directly related to the magnitude of impact forces on structures and hence correlates well with the damage level caused by the tsunami to light buildings. Park et al. (2013) have shown that the magnitude and spatial variability of this metric are strongly affected by details of the interaction of overland flow with the ambient physical environment. This



Fig. 27 Map of tsunami-induced maximum momentum flux ($N \times m$) computed with FNW in 10-m resolution Bethany Beach grid, using results of simulations in 31-m resolution OC-2 grid for the area 4 SMF proxy as forcing along the boundary (Figs. 24, 25)

level of details is not well reproduced in the standard finest 1/3 arc-sec (10 m) NOAA or FEMA DEMs, indicating a continuing need for developing more accurate DEMs and land use information. With those, one could perform even higher-resolution tsunami hazard mapping that could be used for developing zoning regulations at the local level (Yeh et al. 2005).

Similarly, Fig. 28 shows a map of maximum tsunami-induced velocity (m/s), an important factor for navigational hazards during a tsunami, in the heavily traveled Indian River Inlet, DE, computed in the Rehoboth Beach 10-m resolution grid (Fig. 25). Two maps of maximum velocity are presented, one for initially dry land (a) and one for initially wet inland areas (b) (river, pond), which the tsunami inundates. Finally, as a last important metric to quantify coastal tsunami impact, Fig. 29 shows a map of tsunami-induced maximum vorticity (1/s), computed around the heavily traveled Ocean City Inlet, in the 10-m resolution Ocean City model grid. We see that, as a result of the tsunami, large eddies are spawned from the jetties, both offshore and onshore of the inlet. Such rotational flow structures are a hazard for navigation and can persist for a long time, even when the main tsunami inundation has receded.

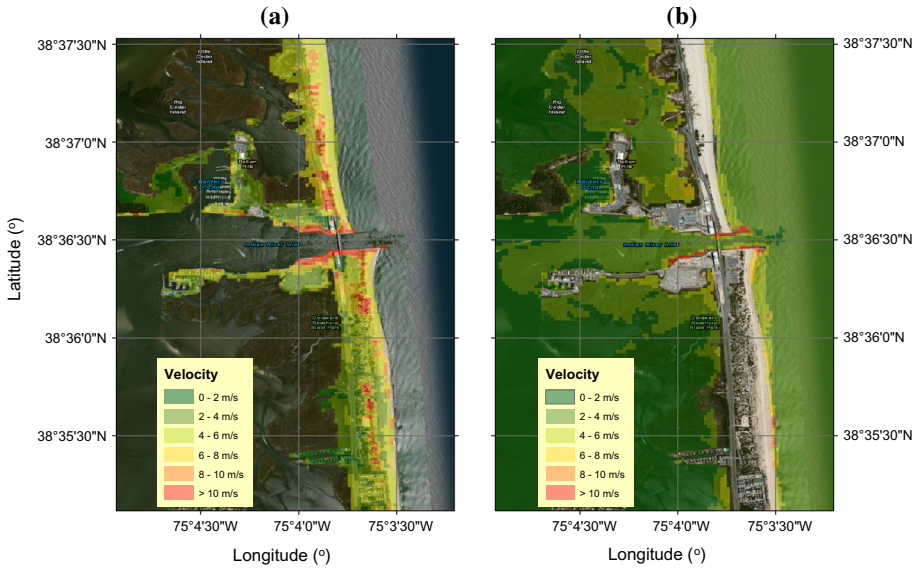
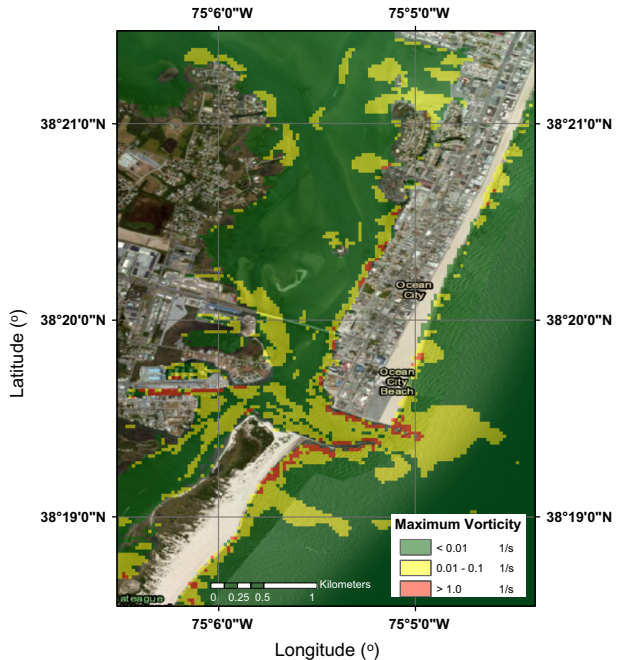


Fig. 28 Maps of tsunami-induced maximum velocity (m/s) computed with FNW around Indian River Inlet, DE, in 10-m resolution Rehoboth Beach, DE grid, using results of simulations in 31-m resolution OC-1 grid for area 4 SMF proxy as forcing along the boundary (Figs. 24, 25): **a** results for initially dry inundated area; **b** results for initially wet inundated area

Fig. 29 Map of tsunami-induced maximum vorticity (1/s) computed with FNW around Ocean City, MD inlet, in 10-m resolution Ocean City grid, using results of simulations in 31-m resolution OC-2 grid for area 4 SMF proxy as forcing along the boundary (Figs. 24, 25)



5 Conclusions

In this paper, we presented both the modeling methodology and results of numerical simulations carried out under the umbrella of the US NTHMP, to develop comprehensive tsunami hazard maps for the upper USEC. While many types of tsunami sources were considered, particularly in the far-field (e.g., Grilli et al. 2010a, b; Abadie et al. 2012; Harris et al. 2012), here we only reported on coastal tsunami hazard associated with near-field tsunamigenic SMF sources.

In such work, the first important aspect was to properly site and parameterize the potentially tsunamigenic sources, here SMFs, that define the PMTs for the considered areas. Then, for each of the selected sources, simulations of tsunami generation and propagation were performed in a series of nested grids with gradually finer resolution, centered on various areas of interest. Based on these, maps of maximum tsunami inundation and other metrics of tsunami hazard (e.g., flow velocity/vorticity, momentum flux) were constructed.

Tsunami simulations were performed using a combination of two state-of-the-art numerical models, which were validated as part of a NTHMP workshop. SMF tsunami generation was simulated using the 3D non-hydrostatic model NHWAVE (NHW; Ma et al. 2012) and subsequent propagation using the fully nonlinear and dispersive 2D Boussinesq model FUNWAVE-TVD in its Cartesian implementation (FNW; Shi et al. 2012). Both models can accurately simulate the more dispersive wavetrains generated by SMFs. After each SMF had stopped moving, simulations in the coarsest FNW grid (500-m resolution grid) were initialized using the surface elevation and horizontal velocity at the required depth computed with NHW. Then, simulations were pursued with FNW in a series of nested grids, based on a one-way coupling methodology. In the latter, simulations in a finer nested grid level are forced by time series of surface elevation and current, computed along its boundary in the coarser grid level (where the entire simulation has also been performed); this way, both incident and reflected waves are included in the time series, which automatically satisfy an open boundary condition.

In the absence of sediment data and information on failure mechanisms, consistent with the PMT approach, SMFs were modeled as rigid slumps, which maximizes tsunami generation, all other parameters being equal (Grilli and Watts 2005); hence, this approach is conservative. As this might be too pessimistic for some situations, in future work, based on field data, we are planning to investigate effects of SMF deformation on tsunami generation, e.g., using the recently extended NHW model (Ma et al. 2013); this could result in smaller tsunami inundation in some areas.

In a preliminary phase to this work, overall SMF tsunami hazard was estimated along the USEC based on Monte Carlo simulations (MCS; Grilli et al. 2009) of slope stability and tsunami generation and impact. These indicated an increased level of SMF tsunami hazard north of Virginia, potentially surpassing the inundation generated by a typical 100-year hurricane storm surge in the region; to the south, SMF tsunami hazard significantly decreased. Subsequent geotechnical and geological analyses (Krauss 2011; Eggeling 2012) delimited four high-risk areas along the upper USEC, which based on field data (i.e., sediment nature and volume/availability), have the potential for large tsunamigenic SMFs.

Pending the acquisition of more detailed geological and geophysical field data, and consistent with the conservative SMF proxy methodology agreed upon by NTHMP investigators, we defined the SMF PMT in the four identified high-risk areas (Fig. 1) as having the same characteristics as the Currituck slide (i.e., a so-called Currituck proxy), which is the largest historical event identified in the region. In future work, once site-

specific field data are available, some of the selected SMF proxies could be revised and a new generation of inundation maps developed based on these.

After an introduction to the problem and a presentation of the tsunami modeling methodology, the second part of the paper was devoted to parameterizing and modeling the historical Currituck SMF event, including: (1) a new reconstruction of the slide geometry and kinematics; (2) the simulation of the resulting tsunami source generation; and (3) the propagation of the tsunami source over the shelf to the coastline; and to assess the accuracy and convergence of various numerical results. For the latter, a sensitivity analysis to model and grid parameters was performed that confirmed the convergence and accuracy of the coupled modeling approach NHW/FNW and tsunami simulation results. Then, to further validate the proposed grid nesting and one-way coupling methodologies in this context, we modeled the impact of the historical Currituck tsunami event along the nearest coastline where its energy was focused. We thus showed that, assuming today's sea level, the brunt of tsunami impact and inundation would have occurred off and south of Virginia Beach, VA, with the tsunami overtopping a large section of the barrier beaches. These results are in qualitative agreement with earlier modeling of the Currituck tsunami (Geist et al. 2009). Additionally, the tsunami would have propagated and refracted into the Chesapeake Bay, causing up to 3 m inundation in Norfolk, VA, inside the Bay.

In a third part, we finally modeled tsunami generation, propagation, and coastal impact from SMF Currituck proxy sources sited in each of the four high-risk areas. Each tsunami source appeared to share many characteristics with the Currituck event, although details differed due to site-specific effects on wave generation and propagation. A full illustration of the SMF tsunami hazard assessment performed in the context of NTHMP along the USEC was finally presented for the Ocean City, MD area, which is highly vulnerable to tsunami inundation, particularly in the summer when its population increases many folds, due to evacuation problems. It was found that due to its southern location, Ocean City was only significantly affected by the Area 4 SMF proxy; this is expected due to the more directional nature of SMF tsunamis, as compared to co-seismic sources (Tappin et al. 2008). Although no details are provided in this paper, simulations for other areas further north would show that these are primarily affected by other SMF proxies.

Complete high-resolution maps (up to 10 m) of maximum inundation, currents, vorticity, and momentum flux, caused by the tsunami generated from the Area 4 SMF proxy, were thus presented for the most impacted areas around Ocean City. A comparison of these results with similar maps corresponding to the far-field tsunamis, not detailed here, indicates that SMF tsunamis represent one of the largest coastal hazards for many coastal communities along the USEC. Similar to hurricane flood maps, tsunami hazard maps, such as developed here, would allow both better defining zoning plans, relative to coastal developments, and mitigating the effects of future tsunamis by way of protective measures and educational programs. At the completion of the NTHMP project, all the final high-resolution maps of inundation and other products, computed for both SMF and other types of tsunami sources (PMTs), will be posted on the NTHMP Web site and available for download.

SMF tsunamis would offer little warning time along the USEC because they: (1) could be triggered by moderate seismic activity that would only be felt locally and (2) would occur close to shore thus having fairly short propagation times. Besides, standard deep-water tsunami gages (e.g., NOAA's DART buoys) would be ineffective in sensing SMF tsunamis propagating toward the nearest shorelines. Hence, early warning systems appropriate to sensing near-field tsunamis should be developed, e.g., based on the high-frequency radar remote sensing. In this respect, SMF tsunami simulations such as

presented here could help in assessing the salient tsunami flow properties to be sensed by such systems, for potentially high-impacted locations.

Acknowledgments This work has been supported by the National Tsunami Hazard Mitigation Program (NTHMP), NOAA, through grant NA10NWS4670010 to the University of Delaware (with subaward to the University of Rhode Island). Additional support at the University of Rhode Island came from grant EAR-09-11499 from the US National Science Foundation, Geophysics Program. Development of the numerical models used in this study was supported by the Office of Naval Research, Littoral Geosciences and Optics program. S. Banihashemi was supported by the Dept. of Civil and Environmental Engineering, Univ. of Delaware.

References

- Abadie S, Morichon D, Grilli ST, Glockner S (2010) Numerical simulation of waves generated by landslides using a multiple-fluid Navier–Stokes model. *Coast Eng* 57:779–794
- Abadie S, Harris JC, Grilli ST, Fabre R (2012) Numerical modeling of tsunami waves generated by the flank collapse of the Cumbre Vieja Volcano (La Palma, Canary Islands): tsunami source and near field effects. *J Geophys Res* 117:C05030
- Amante C, BW Eakins (2009) ETOPO-1 1 arc-minute global relief model: procedures, data sources and analysis. NOAA Tech. Mem. NESDIS NGDC-24
- Barkan R, ten Brink US, Lin J (2009) Far field tsunami simulations of the 1755 Lisbon earthquake: implication for tsunami hazard to the US East Coast and the Caribbean. *Mar Geol* 264:109–122
- Bunn AR, McGregor BA (1980) Morphology of the North Carolina continental slope, Western North Atlantic, shaped by deltaic sedimentation and slumping. *Mar Geol* 37:253–266
- Chaytor J, ten Brink US, Solow J, Andrews BD (2009) Size distribution of submarine landslides along the U.S. Atlantic Margin. *Mar Geol* 264:16–27
- Egging T (2012) Analysis of earthquake triggered submarine landslides at four locations along the U.S. east coast. Masters Thesis. University of Rhode Island
- Enet F, Grilli ST (2007) Experimental study of tsunami generation by three-dimensional rigid underwater landslides. *J Waterw Port Coast Ocean Eng* 133(6):442–454
- Fine IV, Rabinovich AB, Bornhold BD, Thomson R, Kulikov EA (2005) The Grand Banks landslide-generated tsunami of November 18, 1929: preliminary analysis and numerical modeling. *Mar Geol* 215:45–57
- Geist E, Lynett P, Chaytor J (2009) Hydrodynamic modeling of tsunamis from the Currituck landslide. *Mar Geol* 264:41–52
- Grilli ST, Watts P (1999) Modeling of waves generated by a moving submerged body. Applications to underwater landslides. *Eng Anal Bound Elem* 23:645–656
- Grilli ST, Vogelmann S, Watts P (2002) Development of a 3D Numerical Wave Tank for modeling tsunami generation by underwater landslides. *Eng Anal Bound Elem* 26(4):301–313
- Grilli ST, Watts P (2005) Tsunami generation by submarine mass failure, I: modeling, experimental validation, and sensitivity analyses. *J Waterw Port Coast Ocean Eng* 131(6):283–297
- Grilli ST, Ioualalen M, Asavanant J, Shi F, Kirby JT, Watts P (2007) Source constraints and model simulation of the December 26, 2004 Indian Ocean tsunami. *J Waterw Port Coast Ocean Eng* 133:414–428
- Grilli ST, Taylor O-DS, Baxter CDP, Maretzki S (2009) Probabilistic approach for determining submarine landslide tsunami hazard along the upper East Coast of the United States. *Mar Geol* 264(1–2):74–97
- Grilli ST, Dias F, Guyenne P, Fochesato C, Enet F (2010a) Progress in fully nonlinear potential flow modeling of 3D extreme ocean waves, Chapt 3. In: Ma QW (ed) *Advances in numerical simulation of nonlinear water waves*, vol 11 in Series in Advances in Coastal and Ocean Engineering). World Scientific Publishing Co. Pte. Ltd., pp 75–128, ISBN: 978-981-283-649-6
- Grilli ST, Dubosq S, Pophet N, Pérignon Y, Kirby JT, Shi F (2010b) Numerical simulation and first-order hazard analysis of large co-seismic tsunamis generated in the Puerto Rico trench: near-field impact on the north shore of Puerto Rico and far-field impact on the US East Coast. *Nat Hazard Earth Syst Sci* 10:2109–2125. doi:10.5194/nhess-2109-2010
- Grilli ST, Harris J, Tajalli Bakhsh TS (2011) Literature Review of Tsunami Sources Affecting Tsunami Hazard Along the US East Coast. NTHMP Progress report, Res Rept CACR-11-08, Center for Applied Coastal Research, University of Delaware, Newark. <http://chinacat.coastal.udel.edu/papers/grilli-et-al-cacr-11-08.pdf>
- Grilli ST, Harris J, Shi F, Kirby JT, Tajalli Bakhsh TS, Estibals E, Tehranirad B (2013a) Numerical modeling of coastal tsunami dissipation and impact. In: Lynett P, Mc Kee Smith J (eds) *Proceedings of*

- 33rd International Coast Engineering Conference (ICCE12, Santander, Spain, July, 2012), World Sci Pub Co Pte Ltd
- Grilli ST, Harris JC, Tajalli Bakhsh TS, Masterlark TL, Kyriakopoulos C, Kirby JT, Shi F (2013b) Numerical simulation of the 2011 Tohoku tsunami based on a new transient FEM co-seismic source: comparison to far- and near-field observations. *Pure Appl Geophys* 170:1333–1359. doi:[10.1007/s00024-012-0528-y](https://doi.org/10.1007/s00024-012-0528-y)
- Grothe PR, Taylor LA, Eakins BW, Warnken RR, Carignan KS, Lim E, Caldwell RJ, Friday DZ (2010) Digital elevation model of Ocean City, Maryland: procedures, data sources and analysis. NOAA Technical Memorandum NESDIS NGDC-37
- Harris JC, Grilli ST, Abadie S, Tajalli Bakhsh TS (2012) Near- and far-field tsunami hazard from the potential flank collapse of the Cumbre Vieja Volcano. In: Proceedings of 22nd Offshore Polar Engineering Conference (ISOPE12, Rodos, Greece, June 17–22, 2012), International Society of Offshore and Polar Engineers, pp 242–249
- Ioualalen M, Asavanant JA, Kaewbanjak N, Grilli ST, Kirby JT, Watts P (2007) Modeling of the 26th December 2004 Indian Ocean tsunami: case study of impact in Thailand. *J Geophys Res* 112:C07024. doi:[10.1029/2006JC003850](https://doi.org/10.1029/2006JC003850)
- Kirby JT, Shi F, Tehranirad B, Harris JC, Grilli ST (2013) Dispersive tsunami waves in the ocean: model equations and sensitivity to dispersion and Coriolis effects. *Ocean Model* 62:39–55. doi:[10.1016/j.ocemod.2012.11.009](https://doi.org/10.1016/j.ocemod.2012.11.009)
- Krauss T (2011) Probabilistic tsunami hazard assessment for the United States East Coast. Masters Thesis. University of Rhode Island. <http://chinacat.coastal.udel.edu/nthmp/krause-ms-uri11.pdf>
- Locat J, Lee H, ten Brink US, Twichell D, Geist E, Sansoucy M (2009) Geomorphology, stability and mobility of the Currituck slide. *Mar Geol* 264:28–40
- Lynett P, Liu PL-F (2002) A numerical study of submarine landslide generated waves and runup. *Proc R Soc Lond A458*:2885–2910
- Lynett P, Liu PL-F (2005) A numerical study of the run-up generated by three-dimensional landslides. *J Geophys Res* 110:C03006. doi:[10.1029/2004JC002443](https://doi.org/10.1029/2004JC002443)
- Ma G, Shi F, Kirby JT (2012) Shock-capturing non-hydrostatic model for fully dispersive surface wave processes. *Ocean Model* 43–44:22–35
- Ma G, Kirby JT, Shi F (2013) Numerical simulation of tsunami waves generated by deformable submarine landslides. *Ocean Model* 69:146–165
- Park H, Cox DT, Lynett PJ, Wiebe DM, Shin S (2013) Tsunami inundation modeling in constructed environments: a physical and numerical comparison of free-surface elevation, velocity, and momentum flux. *Coast Eng* 79:9–21
- Piper DJW, Cochonat P, Morrison ML (1999) The sequence of events around the epicentre of the 1929 Grand Banks earthquake: initiation of the debris flows and turbidity current inferred from side scan sonar. *Sedimentology* 46:79–97
- Prior DP, Doyle EH, Neurauter T (1986) The Currituck Slide, Mid Atlantic continental slope-revisited. *Mar Geol* 73:25–45
- Schnyder JSD, Kirby JT, Shi F, Tehranirad B, Eberli GP, Mulder T, Ducassou E (2013) Potential for tsunami generation along the western Great Bahama Bank by submarine slope failures. Abstract NH41A-1689, AGU Fall Meeting, San Francisco, December
- Shi F, Kirby JT, Harris JC, Geiman JD, Grilli ST (2012) A high-order adaptive time-stepping TVD solver for Boussinesq modeling of breaking waves and coastal inundation. *Ocean Model* 43–44:36–51
- Tappin DR, Watts P, Grilli ST (2008) The Papua New Guinea tsunami of 1998: anatomy of a catastrophic event. *Nat Hazards Earth Syst Sci* 8:243–266
- Tehranirad B, Shi F, Kirby JT, Harris JC, Grilli ST (2011) Tsunami benchmark results for fully nonlinear Boussinesq wave model FUNWAVE-TVD, Version 1.0. Research Report No. CACR-11-02, Center for Applied Coastal Research Univ of Delaware, Newark
- Tehranirad B, Kirby JT, Ma G, Shi F (2012) Tsunami benchmark results for non-hydrostatic wave model NHWAVE (Version 1.0). Research Report No. CACR-12-03, Center for Applied Coastal Research Univ of Delaware, Newark
- ten Brink US, Twichell D, Geist E, Chaytor J, Locat J, Lee H, Buczkowski B, Barkan R, Solow A, Andrews B, Parsons T, Lynett P, Lin J, Sansoucy M (2008) Evaluation of tsunami sources with the potential to impact the U.S. Atlantic and Gulf coasts. Report to the Nuclear Regulatory Commission. USGS
- ten Brink US, Lee HJ, Geist EL, Twichell D (2009a) Assessment of tsunami hazard to the U.S. East Coast using relationships between submarine landslides and earthquakes. *Mar Geol* 264:65–73
- ten Brink US, Barkan R, Andrews BD, Chaytor JD (2009b) Size distributions and failure initiation of submarine and subaerial landslides. *Earth Planet Sci Lett* 287:31–42

- Twichell DC, Chaytor JB, ten Brink US, Buczkowski B (2009) Morphology of late quaternary submarine landslides along the U.S. Atlantic Continental Margin. *Mar Geol* 264:4–15
- Watts P, Grilli ST, Kirby JT, Fryer GJ, Tappin DR (2003) Landslide tsunami case studies using a Boussinesq model and a fully nonlinear tsunami generation model. *Nat Hazards Earth Syst Sci* 3:391–402
- Watts P, Grilli ST, Tappin DR, Fryer G (2005) Tsunami generation by submarine mass failure, II: predictive equations and case studies. *J Waterw Port Coast Ocean Eng* 131(6):298–310
- Yeh H, Robertson I, Preuss J (2005) Development of design guidelines for structures that serve as tsunami vertical evacuation sites. Open File Rept. 2005-4, Washington Division of Geology and earth Resources